Andreas Feiersinger, BSc

Time Delay Estimation and Compression of Chirp Train Signals

MASTER'S THESIS

to achieve the university degree of

Diplom-Ingenieur

Master's degree programme: Information and Computer Engineering

submitted to

Graz University of Technology

Supervisors

Univ.-Prof. Dipl.-Ing. Dr. Klaus Witrisal, Dipl.-Ing. Andreas Fuchs

Christian Doppler Labor für Ortssensitive Elektronische Systeme

Institut für Kommunikationsnetze und Satellitenkommunikation

Graz, September 07, 2023

This document is set in Palatino, compiled with pdfLaTeX2e and Biber.

The LaTeX template from Karl Voit is based on KOMA script and can be found online: https://github.com/novoid/LaTeX-KOMA-template

AFFIDAVIT

I declare that I have authored this thesis independently, that I have not used other than the declared sources/resources, and that I have explicitly indicated all material which has been quoted either literally or by content from the sources used. The text document uploaded to TUGRAZonline is identical to the present master's thesis.

Signed by:	Andreas Feiersinger
Date:	07.09.2023 03:47:40

This document is digitally signed!

This document bearing a qualified electronic signature has the same legal standing as a handwritten document in accordance with Article 25 (2) of Regulation (EU) No. 910/2014 of 23 July 2014 ("eIDAS-VO").

Validation: Information for checking the electronic signature can be found at: www.a-trust.at/pdf

Date, Signature

Abstract

In this master's thesis, the influence of unknown starting phases of wide-band chirp-train signals on time-delay estimation is investigated for a single transmitter and a single receiver. This influence is examined for the additive white Gaussian noise (AWGN) scenario and also for a dense multipath (DM) environment. The fundamental performance limits for these cases are derived using the Cramér-Rao Lower bound (CRLB) and compared against different estimators using simulations. The estimators include the maximum likelihood (ML) estimator for the AWGN case and an algorithm that aims to find the first path when multiple paths are present. Since the chirp-train signals are very long and therefore have to be processed on a host computer, a chirp compression algorithm is presented that drastically reduces the bandwidth requirements between the receiver and the host computer. This is implemented for a field-programmable gate array (FPGA). Simulations show a significant accuracy decrease if a long chirp signal is split into multiple subchirps. This loss of accuracy is maximum in the AWGN case and minimum if there is significant energy of the DM present in the received signal. Doubling the number of subchirps for the AWGN case, when the bandwidth stays the same, leads to a four times larger CRLB of the time delay estimation and a 6.02 dB decrease of the effective signal-to-noise (SNR) ratio.

Kurzfassung

In dieser Masterarbeit wird der Einfluss unbekannter Startphasen von Breitband Chirp-Train-Signalen auf die Zeitverzögerungsschätzung für einen einzelnen Sender und einen einzelnen Empfänger analysiert. Dieser Einfluss wird sowohl für das Szenario des additiven weißen Gaußschen Rauschens (AWGN) als auch für einen Dense Multipath (DM) untersucht. Die unteren Schranken der Genauigkeiten der Zeitverzögerungsschätzung werden in diesen Fällen mithilfe der Cramér-Rao Lower Bound (CRLB) hergeleitet und anhand von Simulationen mit verschiedenen Schätzern verglichen. Die Schätzmethoden umfassen den Maximum-Likelihood-Schätzer (ML) für den AWGN-Fall sowie einen Algorithmus zur Schätzung des ersten Pfades, wenn mehrere Pfade vorliegen, wie im DM-Szenario. Aufgrund der erheblichen Länge der Chirp-Train-Signale wird ein Chirp-Kompressionsalgorithmus präsentiert, der die Bandbreitenanforderungen zwischen dem Empfänger und dem Host-Computer erheblich minimiert welcher auf einem Field-Programmable Gate Array (FPGA) implementiert wird. Wenn ein langes Chirp-Signal in mehrere Subchirps aufgeteilt wird, resultiert dies in einem deutlichen Genauigkeitsverlust, wie durch Simulationen bestätigt wurde. Im AWGN-Fall ist der Genauigkeitsverlust am größten und wenn das empfangene Signal eine signifikante Energie im DM aufweist ist dieser am geringsten. Die Verdoppelung der Anzahl der Subchirps im AWGN-Fall führt bei gleicher Bandbreite zu einer viermal größeren CRLB der Zeitverzögerungsschätzung und zu einer Verringerung des effektiven Signal-Rausch-Verhältnisses (SNR) um 6,02 dB.

Contents

List of Figures

1 Introduction

The estimation of the time delay is the basis for accurate positioning in wireless networks and many other areas of signal processing. In positioning, the distances from the receiver node to given transmitter nodes are calculated by estimating the propagation delays of the transmitted signals and then converting them to distances using the speed of electromagnetic waves [1]. The position can then be calculated by using the multilateration principle which requires at least three distances. The best-known positioning system is perhaps the Global Positioning System (GPS). Indoor positioning is an alternative to GPS for environments where it is not effective, such as enclosed spaces, and is essential for indoor navigation and location awareness of autonomous drones and IoT devices. Indoor positioning usually needs to be more accurate than GPS, but this is often difficult due to multipath propagation, for example, caused by obstacles. Time delay estimation is also crucial for estimating distances in radar applications.

The bandwidth of the transmitted signals plays a major role in time delay estimation. Chirp signals are a popular and inexpensive method to generate signals with a desired bandwidth, which is why they can be used for this purpose. These chirps can be generated for example by direct digital synthesis (DDS) [2] or by manipulating registers of a radio chip as done in [3]. In the second case, the radio chip supports a bandwidth of up to 80 MHz which, if utilized, allows a much more accurate time delay estimation than narrowband signals. Due to the limitation of some radio chips that a chirp can cover a limited bandwidth only, a chirp-train signal must be generated to utilize the full bandwidth. A chirp train or stepped chirp is a coherent sequence of different chirp signals which are called subchirps. The concept of a chirp-train generation for increasing the time delay accuracy has already been shown in [4]. However, the approach from [3] introduces unknown start phases for each subchirp.

Because of that and due to the large amount of data the chirp train causes, more complicated algorithms are required for estimating the time delay and larger memories are needed. Usually, the memory on the receiver chips is not sufficient, therefore the samples have to be sent to the host computer as soon as they are received.

For the estimation of the time delay, a lower bound is usually defined on the accuracy. This allows an evaluation of the accuracy of different estimators since the closer this accuracy is to the bound, the better the estimator is. The influence of an unknown start phase of a signal on the theoretical lower bound for the time delay estimation given by the Cramér-Rao Lower bound (CRLB) is a well-known result [5]. This refers to the Additive white Gaussian noise (AWGN) case when there is a single line of sight component (LOS) only. Furthermore, this analysis has been extended for the Dense Multipath (DM) case in [6] where several differently scaled and time-delayed components arrive at the receiver and interfere with each other.

This work aims to extend these concepts for the case of a chirp-train signal where all start phases are unknown and to derive a theoretical lower bound given by the CRLB. This allows a better understanding of how much the time delay estimate is affected by unknown start phases of the subchirps. A key question is how the time delay estimation is affected when a chirp-train signal with unknown start phases is used instead of one single chirp with the same total bandwidth. Furthermore, estimation methods for the AWGN and the DM cases are presented. For the validation of the CRLB and the analysis under which conditions the estimators reach the CRLB and which estimator can perform best, simulations are created. Due to the high bandwidth and the resulting transmission difficulties from the receiver to the host computer, a chirp compression algorithm is described. The implementation details of this algorithm are shown for a software-defined radio (SDR) as the receiver, which is equipped with a field-programmable gate array (FPGA) for real-time signal processing.

This thesis has the following structure:

2. **Theory**: Mathematical methods that are used throughout the thesis are introduced.

3. **Signal Model**: The chirp-train signal model and the received signal models for the AWGN and the DM cases are defined.

4. **FPGA Implementation of the Chirp Compression Algorithm**: The used FPGA is described, the chirp compression algorithm is explained and implementation details on the FPGA are shown.

5. **Cramér–Rao Lower Bound for Time Delay Estimation**: In this chapter, the CRLBs for the AWGN and the DM cases are derived for chirp-train signals.

6. **Time Delay Estimation and Algorithms**: Time delay estimation algorithms for the AWGN and the DM cases are described in this chapter.

7. **Simulations**: Simulations of the CRLBs and the estimation methods are carried out.

8. **Conclusion**

2 Theory

2.1 Cramér-Rao Lower Bound

The Cramér-Rao Lower Bound (CRLB) is the theoretical lower bound for the variance of unbiased estimators and therefore it can be used for performance evaluations. If an unbiased estimator achieves the CRLB it is called a minimum variance unbiased (MVU) estimator [5]. For a probability density function (PDF) $p(\boldsymbol{x};\boldsymbol{\theta})$ where $\boldsymbol{x} \in \mathbb{C}^M$ is the data vector of length M and $\boldsymbol{\theta} \in \mathbb{R}^K$ is the unknown parameter vector with K parameters, the regularity condition is defined as

$$\mathbb{E}\left[\frac{\partial \ln p(\boldsymbol{x};\boldsymbol{\theta})}{\partial \boldsymbol{\theta}}\right] = \mathbf{0} \,. \tag{2.1}$$

If this regularity condition holds, the element of the i-th row and j-th column of the Fisher information matrix (FIM) can be calculated as

$$[\boldsymbol{\mathcal{I}}(\boldsymbol{\theta})]_{ij} = -\mathbb{E}\left[\frac{\partial^2 \ln p(\boldsymbol{x};\boldsymbol{\theta})}{\partial\theta_i \partial\theta_j}\right] \quad \text{for} \quad 0 \leq i,j \leq K-1 \,. \tag{2.2}$$

The CRLB for the i-th parameter is then given by

$$\operatorname{var}(\hat{\theta}_i) \geq [\boldsymbol{I}^{-1}(\boldsymbol{\theta})]_{ii} \,, \tag{2.3}$$

which means that the CRLB of a parameter is bounded by the corresponding element of the inverse FIM [5]. For the complex Gaussian case with

$$\boldsymbol{x} \sim \mathcal{CN}(\boldsymbol{\mu}(\boldsymbol{\theta}), \boldsymbol{C}(\boldsymbol{\theta})) \,, \tag{2.4}$$

where $\boldsymbol{\mu}(\boldsymbol{\theta}) \in \mathbb{C}^M$ is the mean vector and $\boldsymbol{C}(\boldsymbol{\theta}) \in \mathbb{C}^{M \times M}$ is the covariance matrix, the element of the i-th row and j-th column of the FIM can be calculated as [5]

$$[\boldsymbol{I}(\boldsymbol{\theta})]_{ij} = 2\,\mathrm{Re}\left\{ \left(\frac{\partial \boldsymbol{\mu}(\boldsymbol{\theta})}{\partial \theta_i} \right)^H \boldsymbol{C}^{-1}(\boldsymbol{\theta}) \frac{\partial \boldsymbol{\mu}(\boldsymbol{\theta})}{\partial \theta_j} \right\} + \mathrm{tr}\left[\boldsymbol{C}^{-1}(\boldsymbol{\theta}) \frac{\partial \boldsymbol{C}(\boldsymbol{\theta})}{\partial \theta_i} \boldsymbol{C}^{-1}(\boldsymbol{\theta}) \frac{\partial \boldsymbol{C}(\boldsymbol{\theta})}{\partial \theta_j} \right] . \quad (2.5)$$

For the AWGN case with covariance matrix $\boldsymbol{C}(\boldsymbol{\theta}) = \sigma^2 \boldsymbol{I}_M$, where $\boldsymbol{I}_M$ is the M-dimensional identity matrix, Equation (2.5) can be simplified to

$$[\boldsymbol{\mathcal{I}}(\boldsymbol{\theta})]_{ij} = \frac{2}{\sigma^2}\,\mathrm{Re}\left\{ \left(\frac{\partial \boldsymbol{\mu}(\boldsymbol{\theta})}{\partial \theta_i} \right)^H \frac{\partial \boldsymbol{\mu}(\boldsymbol{\theta})}{\partial \theta_j} \right\} . \quad (2.6)$$

2.2 Maximum Likelihood Estimation for the Gaussian Case

The maximum likelihood (ML) estimator is a popular approach to obtain parameter estimates for nonlinear models since it provides a cost function for which an optimum with respect to the parameters can be found. For linear models, the ML estimate is equal to the MVU and even for nonlinear models it often is asymptotically efficient [5].

First of all a Gaussian distributed random vector is considered

$$\boldsymbol{r} = \boldsymbol{\mu}(\boldsymbol{\theta}) + \boldsymbol{w} \,, \tag{2.7}$$

with a parameter vector $\boldsymbol{\theta} \in \mathbb{R}^K$, a mean vector $\boldsymbol{\mu}(\boldsymbol{\theta})$ and a covariance matrix $\boldsymbol{C}_w$ that is independent of $\boldsymbol{\theta}$. The PDF is written as

$$p(\boldsymbol{r};\boldsymbol{\theta}) \propto \exp\left(-\frac{1}{2}\left(\boldsymbol{r}-\boldsymbol{\mu}(\boldsymbol{\theta})\right)^H \boldsymbol{C}_w^{-1}\left(\boldsymbol{r}-\boldsymbol{\mu}(\boldsymbol{\theta})\right)\right) \,. \tag{2.8}$$

The optimum with respect to the parameter vector $\boldsymbol{\theta}$ can be found as

$$\begin{aligned}
\hat{\boldsymbol{\theta}} &= \arg\max_{\boldsymbol{\theta}} \left\{p(\boldsymbol{r};\boldsymbol{\theta})\right\} && \text{(2.9a)}\\
&= \arg\max_{\boldsymbol{\theta}} \left\{\ln p(\boldsymbol{r};\boldsymbol{\theta})\right\} && \text{(2.9b)}\\
&= \arg\min_{\boldsymbol{\theta}} \left\{\left(\boldsymbol{r}-\boldsymbol{\mu}(\boldsymbol{\theta})\right)^H \boldsymbol{C}_w^{-1}\left(\boldsymbol{r}-\boldsymbol{\mu}(\boldsymbol{\theta})\right)\right\} \,. && \text{(2.9c)}
\end{aligned}$$

When the model is a linear one with respect to the parameter vector $\boldsymbol{\theta}$ i.e.

$$\boldsymbol{\mu}(\boldsymbol{\theta}) = \boldsymbol{A}\boldsymbol{\theta} \,, \tag{2.10}$$

with a known matrix $\boldsymbol{A} \in \mathbb{C}^{M\times K}$, the minimization of Equation (2.9c) is achieved by using the Gauss-Markov Theorem [5]. This leads to the parameter estimate

$$\hat{\boldsymbol{\theta}} = \left(\boldsymbol{A}^H\boldsymbol{C}^{-1}\boldsymbol{A}\right)^{-1}\boldsymbol{A}^H\boldsymbol{C}^{-1}\boldsymbol{r} \,, \tag{2.11}$$

which is an MVU estimator for this scenario. For the AWGN case with the covariance matrix $\boldsymbol{C} = \sigma^2 \boldsymbol{I}_M$, Equation (2.11) simplifies to

$$\hat{\boldsymbol{\theta}} = \left(\boldsymbol{A}^H \boldsymbol{A}\right)^{-1} \boldsymbol{A}^H \boldsymbol{r} \,. \tag{2.12}$$

2.3 Discrete Fourier Transformation Matrix

Similar to [7] a unitary discrete Fourier transformation (DFT) matrix is defined as

$$\boldsymbol{W} = \left[\boldsymbol{w}_{-\frac{M}{2}} \,,\, \boldsymbol{w}_{-\frac{M}{2}+1} \,,\, \dots \,,\, \boldsymbol{w}_{\frac{M}{2}-1}\right]^T \,, \tag{2.13}$$

with the vector entries

$$\begin{aligned} \boldsymbol{w}_k = \frac{1}{\sqrt{M}} \Bigg[&\exp\left(-\frac{j2\pi}{M} k0\right) \,,\, \exp\left(-\frac{j2\pi}{M} k1\right) \,, \\ &\dots \,,\, \exp\left(-\frac{j2\pi}{M} k\,(M-1)\right)\Bigg] \,, \end{aligned} \tag{2.14}$$

where M is the total length of the signal and the index k ranges $\frac{M}{2} \leq k \leq \frac{M}{2} - 1$. It should be noted that the inverse of $\boldsymbol{W}$ can be calculated as

$$\boldsymbol{W}^H = \boldsymbol{W}^{-1} \,. \tag{2.15}$$

3 Signal Model

In this chapter, the mathematical model of the transmitted chirp train signal is defined. Furthermore, the received signal models for the additive white Gaussian noise (AWGN) channel and the dense multipath (DM) propagation channel are defined when there is one receiver and one transmitter.

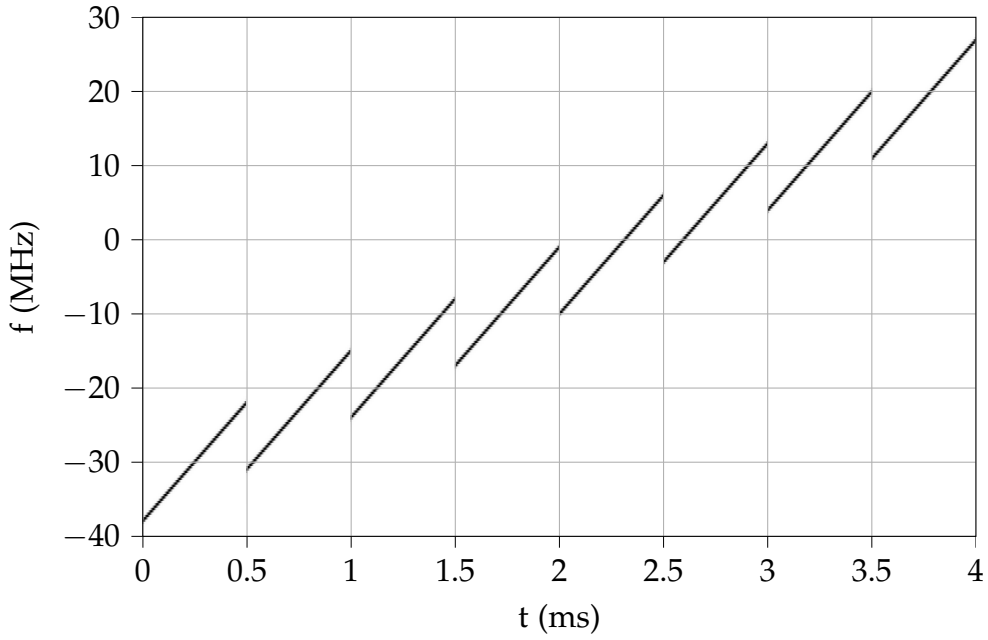

Figure 3.1: Example of a spectrogram of a baseband chirp train signal.

Figure 3.1 shows a spectrogram of a chirp train signal with eight subchirps. In this case, each subchirp has a different starting frequency. The length and the chirp rate of each subchirp are the same.

3.1 Chirp Train Signal

The instantaneous frequency of the i-th subchirp with the starting frequency f_i and the chirp rate c is expressed as

$$f_i(t) = ct + f_i \,, \tag{3.1}$$

where the index ranges $0 \leq i < P$ and P is the amount of subchirps. The instantaneous phase of the i-th subchirp is the integral of the instantaneous frequency plus a starting phase ϕ_i:

$$\begin{aligned} \phi_i(t) &= \phi_i + 2\pi \int_0^t f(t)dt && \text{(3.2a)} \\ &= \phi_i + 2\pi \int_0^t (ct + f_i)dt && \text{(3.2b)} \\ &= \phi_i + 2\pi \left(\frac{ct^2}{2} + f_i t \right) \,. && \text{(3.2c)} \end{aligned}$$

The i-th chirp signal is written as

$$\begin{aligned} s_i(t) &= \exp(j\phi_i(t)) && \text{(3.3a)} \\ &= \exp\left(j\phi_i + j2\pi \left(\frac{ct^2}{2} + f_i t \right) \right) \,. && \text{(3.3b)} \end{aligned}$$

A corresponding sampled version of $s_i(t)$ can be expressed as

$$\begin{aligned} s_i[n] = s_i(nT_s) &= \exp(j\phi_i[n]) && \text{(3.4a)} \\ &= \exp\left(j\phi_i + j2\pi \left(\frac{c\ (nT_s)^2}{2} + f_i n T_s \right) \right) \,, && \text{(3.4b)} \end{aligned}$$

where the sample index ranges $0 \leq n < N_c$, N_c is the length of each subchirp and T_s is the sampling period. Substituting with the sampling frequency normalized chirp rate $m = cT_s$ leads to

$$\begin{aligned} s_i[n] &= \exp\left(j\phi_i + j2\pi T_s \left(\frac{mn^2}{2} + f_i n \right) \right) && \text{(3.5a)} \\ &= \exp\left(j2\pi T_s \left(\frac{mn^2}{2} + f_i n \right) \right) \exp(j\phi_i) && \text{(3.5b)} \\ &= x_i[n] p_i \,, && \text{(3.5c)} \end{aligned}$$

where

$$x_i[n] = \exp\left(j2\pi T_s \left(\frac{mn^2}{2} + f_i n\right)\right) , \tag{3.6}$$

is the i-th subchirp signal without an initial phase shift and

$$p_i = \exp(j\phi_i) , \tag{3.7}$$

is the i-th initial phase shift term.

For the representation of the chirp train a vector notation is used. First of all, the chirp signal $x_i[n]$ is written in the vector form

$$\boldsymbol{x}_i = \left[\mathbf{0}_{1\times iN_c}, x_i[0], x_i[1], \ldots, x_i[N_c-1], \mathbf{0}_{1\times(L+N_c(P-i-1))}\right]^T , \tag{3.8}$$

where $\mathbf{0}_{1\times iN_c}$ and $\mathbf{0}_{1\times(L+N_c(P-i-1))}$ are $1 \times iN_c$ and $1 \times (L + N_c(P - i - 1))$ dimensional zero vectors which are used for padding the individual subchirps such that

$$\boldsymbol{x} = \sum_{i=0}^{P-1} \boldsymbol{x}_i . \tag{3.9}$$

Additionally, L zeros are appended to provide space for the time-shifting operation which is used later in this chapter. The vector form which contains all phase-shifted subchirps is given by

$$\boldsymbol{s} = \boldsymbol{X}\boldsymbol{p} , \tag{3.10}$$

where

$$\boldsymbol{X} = [\boldsymbol{x}_0, \boldsymbol{x}_1, \ldots, \boldsymbol{x}_{P-1}] , \tag{3.11}$$

is the stacked representation of the individual vectors from Equation (3.8) and

$$\boldsymbol{p} = [p_0, p_1, \ldots, p_{P-1}]^T , \tag{3.12}$$

is the vector which contains all phase terms. Furthermore, the matrix representation of the chirp train vector $\boldsymbol{s}$ where the i-th column contains the phase shifted subchirp $\boldsymbol{x}_i p_i$ is defined as

$$\boldsymbol{S} = \boldsymbol{X}\,\mathrm{diag}(\boldsymbol{p})\ , \tag{3.13}$$

where the diagonal matrix $\mathrm{diag}(\boldsymbol{p})$ has the diagonal entries

$$[\mathrm{diag}(\boldsymbol{p})]_{ii} = p_i\ . \tag{3.14}$$

The time derivative of the i-th subchirp can be expressed as

$$\begin{aligned}\dot{x}_i(t) &= \frac{d}{dt}\exp\left(j2\pi\left(\frac{ct^2}{2} + f_i t\right)\right) && \text{(3.15a)}\\ &= j2\pi(ct + f_i)\exp\left(j2\pi\left(\frac{ct^2}{2} + f_i t\right)\right) && \text{(3.15b)}\\ &= j2\pi(ct + f_i)x_i(t)\ . && \text{(3.15c)}\end{aligned}$$

Sampling the time derivative signal $\dot{x}_i(t)$ leads to

$$\begin{aligned}\dot{x}_i[n] &= \dot{x}_i(t)|_{nT_s} && \text{(3.16a)}\\ &= j2\pi(mn + f_i)x_i[n]\ . && \text{(3.16b)}\end{aligned}$$

A similar representation as in Equation (3.10) can be found

$$\dot{\boldsymbol{s}} = \dot{\boldsymbol{X}}\boldsymbol{p}\ , \tag{3.17}$$

using the time derivative matrix

$$\dot{X} = [\dot{\boldsymbol{x}}_0, \dot{\boldsymbol{x}}_1, \ldots, \dot{\boldsymbol{x}}_{P-1}]\ , \tag{3.18}$$

with the entries of the time derivative vector as

$$\dot{\boldsymbol{x}}_i = \left[\mathbf{0}_{1xiN_c}, \dot{x}_i[0], \dot{x}_i[1], \ldots, \dot{x}_i[N_c - 1], \mathbf{0}_{1x(L+N_c(P-i-1))}\right]^T\ , \tag{3.19}$$

such that the time derivative vector $\dot{\boldsymbol{x}}$ is written as

$$\dot{\boldsymbol{x}} = \sum_{i=0}^{P-1} \dot{\boldsymbol{x}}_i\ . \tag{3.20}$$

Similar to Equation (3.13) the matrix representation of the derivative chirp train vector $\dot{\boldsymbol{s}}$ is defined as

$$\dot{\boldsymbol{S}} = \dot{\boldsymbol{X}}\,\mathrm{diag}(\boldsymbol{p})\ . \tag{3.21}$$

3.2 AWGN Channel

In environments where only a LOS component is present the received signal is a time-delayed and scaled version of the transmitted one. Furthermore, additive white Gaussian noise is added. The channel impulse response is written as

$$h(t) = \alpha\delta(t-\tau)\ , \tag{3.22}$$

with the LOS channel coefficient $\alpha \in \mathbb{C}$ and time delay $\tau \in \mathbb{R}$. The received signal is expressed as

$$\begin{aligned} r(t) &= h(t) * s(t) + w(t) && (3.23)\\ &= \alpha s(t-\tau) + w(t)\ , && (3.24) \end{aligned}$$

where $w(t)$ is complex Gaussian noise with power spectral density N_0. Sampling with a sampling period of T_s gives

$$r[n] = \alpha s(nT_s - \tau) + w[n]\ . \tag{3.25}$$

It is assumed that the signal is band-limited between $-f_s/2$ and $f_s/2$ and therefore, $w[n] \sim \mathcal{CN}(0, N_0 f_s)$. A compact vector notation is achieved by combining Equations (3.10) and (3.25) similar to [7, 8]:

$$\boldsymbol{r} = \alpha \boldsymbol{W}^H \boldsymbol{P}(\tau) \boldsymbol{W} \boldsymbol{X} \boldsymbol{p} + \boldsymbol{w}\ , \tag{3.26}$$

where

$$\boldsymbol{P}(\tau) = \operatorname{diag}\left(\left[e^{j\frac{2\pi}{M} k \tau f_s} \right]_{k=-\frac{M}{2}}^{\frac{M}{2}-1} \right)\ , \tag{3.27}$$

is a diagonal matrix, the total length $M = N + L$ of the zero-padded chirp-train signal is assumed to be even and $N = PN_c$ is the chirp-train length. The operator $\operatorname{diag}\left([f(k)]_{k=k_0}^{k_1} \right)$ indicates that the diagonal entries range from $f(k_0)$, $f(k_0+1)$ to $f(k_1)$ and $f : \mathbb{Z} \to \mathbb{C}$ is an arbitrary function.

In Equation (3.26) the signal is transformed into the frequency domain using the unitary DFT matrix $\boldsymbol{W}$ from Equation (2.13), then multiplied with a linear phase matrix $\boldsymbol{P}(\tau)$ for the time delay and finally transformed back

using the inverse of the DFT matrix $\boldsymbol{W}^{-1} = \boldsymbol{W}^{H}$. The signal model assumes that the phases for each subchirp are known and therefore $\boldsymbol{p}$ is known.

A second signal model is defined where the phases for all subchirps are unknown. Since the phase vector $\boldsymbol{p}$ already accounts for phase shifts of the signal, the LOS channel coefficient α simplifies to $|\alpha|$. Therefore, the received signal can be written as

$$\boldsymbol{r} = |\alpha| \boldsymbol{W}^{H} \boldsymbol{P}(\tau) \boldsymbol{W} \boldsymbol{X} \boldsymbol{p} + \boldsymbol{w} \, . \tag{3.28}$$

3.3 Dense Multipath

In real-world environments, the transmitted signal arrives due to multiple propagation paths as a sum of time-delayed and scaled versions at the receiver [9]. Multipath propagation happens because

- Reflection,
- Diffraction and
- Scattering

cause a superposition of the transmitted waves. Furthermore, the multipath propagation changes with different obstacles and positions of the receiver in space. The time shift of the carrier signal leads to a phase shift of the signal at the receiver, which is modeled by channel coefficients that are complex-valued in general.

The high time resolution and the resulting high bandwidth of ultra wideband (UWB) signals allow that multipath components can be resolved [1]. This happens because the length of the compressed received signal after the matched filtering is smaller than the time delay between the individual components of the channel impulse response. In this section, the focus is on signals with a much smaller bandwidth where the length of the compressed received signal is much larger and the multipath components are not separable anymore. Similar to [6, 10], the received signal is described as

$$r(t) = \alpha s(t - \tau) + (s * \nu)(t) + w(t) \, . \tag{3.29}$$

The first term in Equation (3.29) is the deterministic LOS component which is similar to Equation (3.25) in the AWGN case and the second term describes the dense multipath (DM) process where $\nu(t) \in \mathbb{C}$ is a stochastic process that models the multipath components. An advantage of modeling the multipath components as a stochastic process is that it does not only apply to a specific realization of the process such as presented in [8].

The stochastic process $\nu(t)$ is described using the power delay profile $S_\nu(t-\tau)$ and the uncorrelated scattering assumption [11] where

$$\mathbb{E}[\nu(t_2)\nu^*(t_1)] = S_\nu(t_1-\tau)\delta(t_2-t_1)\,, \tag{3.30}$$

which means that the process is uncorrelated when $t_1 \neq t_2$ and therefore $\nu(t) \sim \mathcal{CN}(0, S_\nu(t-\tau))$. Under the assumption that the sampling frequency f_s is larger than the bandwidth of the transmitted signal and the DM process, Equation (3.29) can be time discretized as

$$r[n] = \alpha s(nT_s - \tau) + T_s(s * v)[n] + w[n]\,. \tag{3.31}$$

Similar to Equation (3.26), Equation (3.31) is put into vector notation for compactness:

$$\begin{aligned} \boldsymbol{r} &= \alpha \boldsymbol{W}^H \boldsymbol{P}(\tau)\boldsymbol{W}\boldsymbol{s} + T_s\bar{\boldsymbol{S}}\boldsymbol{\nu} + \boldsymbol{w} && \text{(3.32a)} \\ &= \alpha \boldsymbol{W}^H \boldsymbol{P}(\tau)\boldsymbol{W}\boldsymbol{s} + \boldsymbol{n} \in \mathbb{C}^M\,, && \text{(3.32b)} \end{aligned}$$

where $M = N + L$ is the amount of the received samples, L is the length of the DM process, $\boldsymbol{\nu}$ is a realization of the DM process, $\boldsymbol{n}$ is the sum of the two processes,

$$\bar{\boldsymbol{S}} = [\bar{\boldsymbol{s}}_0, \bar{\boldsymbol{s}}_1, \ldots, \bar{\boldsymbol{s}}_{M-1}]^T \in \mathbb{C}^{MxL}\,, \tag{3.33}$$

is the convolution matrix [11, 12] with entries

$$\bar{\boldsymbol{s}}_i = [s[i], s[i-1], \ldots, s[i-L+1]]\,. \tag{3.34}$$

where $s[i] = 0$ for $i < 0$.

Similar to Equation (3.28) a second signal model, where the phase vector p is unknown and the LOS channel coefficient α simplifies to $|\alpha|$, is defined as

$$\boldsymbol{r} = |\alpha|\boldsymbol{W}^H \boldsymbol{P}(\tau)\boldsymbol{W}\boldsymbol{s} + \boldsymbol{n}\,. \tag{3.35}$$

It is well known that the addition of two zero-mean Gaussian random vectors leads to another zero-mean Gaussian random vector with a different covariance matrix. Therefore, the noise vector is distributed as

$$\boldsymbol{n} \sim \mathcal{CN}(0, \boldsymbol{C}_n) \ , \tag{3.36}$$

with the covariance matrix $\boldsymbol{C}_n$ being defined as

$$\begin{aligned} \boldsymbol{C}_n &= \mathbb{E}[(T_s\bar{\boldsymbol{S}}\boldsymbol{\nu} + \boldsymbol{w})(T_s\bar{\boldsymbol{S}}\boldsymbol{\nu} + \boldsymbol{w})^H] && \text{(3.37a)} \\ &= T_s^2\boldsymbol{S}\mathbb{E}[\boldsymbol{\nu}\boldsymbol{\nu}^H]\bar{\boldsymbol{S}}^H + \mathbb{E}[\boldsymbol{w}\boldsymbol{w}^H] + 2T_s \operatorname{Re}\left\{\bar{\boldsymbol{S}}\underbrace{\mathbb{E}[\boldsymbol{\nu}\boldsymbol{w}^H]}_{0}\right\} && \text{(3.37b)} \\ &= T_s^2\bar{\boldsymbol{S}}\boldsymbol{C}_\nu\bar{\boldsymbol{S}}^H + \frac{N_0}{T_s}\boldsymbol{I}_M \ , && \text{(3.37c)} \end{aligned}$$

with the M-dimensional identity matrix $\boldsymbol{I}_M$. The covariance matrix of the DM process which contains the PDP $S_\nu(t)$ is defined as

$$\boldsymbol{C}_\nu = \operatorname{diag}\left(\left[S_\nu(kT_s - \tau)\right]_{k=0}^{L-1}\right) \ , \tag{3.38}$$

where L is the length of the process noise $\boldsymbol{\nu}$. It should be noted that Equation (3.37b) simplifies to Equation (3.37c) due to the random vectors $\boldsymbol{\nu}$ and $\boldsymbol{w}$ being uncorrelated.

A double-exponential PDP is used similarly to [11]:

$$S_\nu(t-\tau) = \begin{cases} \Omega_1\left(1 - \exp\left(-\frac{t-\tau}{\gamma_r}\right)\right)\exp\left(-\frac{t-\tau}{\gamma_d}\right), & \text{if } t \geq \tau \\ 0, & \text{otherwise} \ , \end{cases} \tag{3.39}$$

where Ω_1 is an energy normalization factor. When the PDP and the LOS components are normalized, Ω_1 describes the energy ratio of the LOS and the PDP. The parameters γ_r and γ_d specify how fast the double exponential function rises and decays.

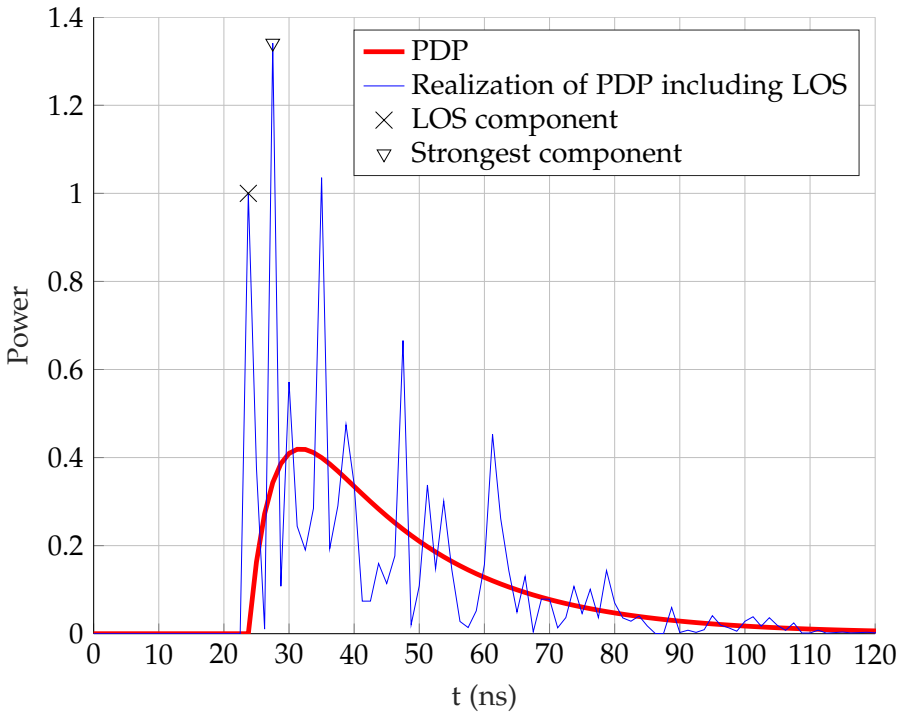

Figure 3.2: Example of a double exponential PDP with $\gamma_r = 5$ ns and $\gamma_d = 20$ ns similar to [11]. A sample rate of 80 MHz and an oversampling factor of 10 has been used.

Figure 3.2 shows an example of a double-exponential PDP including the power of a single realization of the impulse response of the DM process together with the power of the LOS component. Furthermore, the PDP has been normalized such that a discrete convolution with the signal leads to a ten times higher energy in the DM components than in the LOS component. It can be seen that for this case the LOS component is not the strongest one.

The average energy of the DM components can be obtained as

$$\mathbb{E}\Big[\sum_{n=0}^{M-1}|T_s(s*\nu)[n]|^2\Big] = T_s^2\sum_{n=0}^{M-1}\mathbb{E}\Big[|\sum_{k=0}^{\infty}s[n-k]\nu[k]|^2\Big] \tag{3.40a}$$

$$= T_s^2\sum_{n=0}^{M-1}\mathbb{E}\Big[\sum_{k_1=0}^{\infty}s^*[n-k_1]\nu^*[k_1]\sum_{k_2=0}^{\infty}s[n-k_2]\nu[k_2]\Big] \tag{3.40b}$$

$$= T_s^2\sum_{n=0}^{M-1}\sum_{k_1=0}^{\infty}\sum_{k_2=0}^{\infty}s^*[n-k_1]s[n-k_2]\mathbb{E}\Big[\nu^*[k_1]\nu[k_2]\Big] \tag{3.40c}$$

$$= T_s^2\sum_{n=0}^{M-1}\sum_{k=0}^{\infty}|s[n-k]|^2S_\nu[k] \tag{3.40d}$$

$$= T_s^2\sum_{n=0}^{M-1}(p_s*S_\nu)[n]\,, \tag{3.40e}$$

where $p_s[n] = |s[n]|^2$ is the signal power at the sample index n. It should be noted that Equation (3.40c) simplifies to Equation (3.40d) because of the uncorrelated scattering assumption from Equation (3.30). Due to the squaring of the magnitude, the summation indices k_1 and k_2 are used in Equation (3.40b) instead of the index k in Equation (3.40a),

When a chirp train signal model is used

$$|p_s[n]|^2 = 1 \quad \text{for} \quad 0 \le n \le N-1\,, \tag{3.41}$$

and the assumption is used that N is much larger than L such that $M \approx N$ Equation (3.40e) can be approximated:

$$\mathbb{E}\Big[\sum_{n=0}^{M-1}|T_s(s*\nu)[n]|^2\Big] \approx T_s^2 N\sum_{k=0}^{\infty}S_\nu[k]\,. \tag{3.42}$$

Similar to [13] the Rician K-factor is defined as

$$K_{\text{LOS}} = \frac{|\alpha|^2\sum_{n=0}^{N-1}|s[n]|^2}{\mathbb{E}\Big[|T_s(s*\nu)[n]|^2\Big]} \tag{3.43a}$$

$$= \frac{|\alpha|^2 N}{T_s^2\sum_{n=0}^{M-1}(p_s*S_\nu)[n]}\,, \tag{3.43b}$$

which gives the average ratio between the received energy present in the LOS component and the DM. Using the above assumptions for the chirp train signal and the approximation from Equation (3.42), Equation (3.43b) can be simplified to

$$K_{LOS} = \frac{|\alpha|^2}{T_s^2 \sum_{k=0}^{\infty} S_v[k]} \tag{3.44a}$$

$$= \frac{|\alpha|^2}{T_s \Omega_1} \,, \tag{3.44b}$$

with the energy normalization factor of the PDP

$$\Omega_1 = \sum_{k=0}^{\infty} S_v[k] T_s \,. \tag{3.45}$$

4 FPGA Implementation of the Chirp Compression Algorithm

4.1 Overview

As seen in [3], it is possible to generate a signal bandwidth up to 80 MHz which is centered at 2.4 Ghz using a Texas Instruments CC2510 transceiver chip. This approach allows to generate wideband signals using narrowband transmitters which is essential for a low-cost and accurate time delay estimation and positioning. The CC2510 transceiver chip consists of a phase-locked loop (PLL) based frequency synthesizer which can be programmed to generate frequency chirp signals for a specific bandwidth. In [3] this is done by setting the registers:

- CHANSPC (8 bit) which specifies the chirp steepness.
- FREQ (24 bit) which specifies the start frequency of the chirp.
- CHAN which is incremented or decremented continuously to achieve the frequency ramp.

However, a chirp can only cover a bandwidth of up to 12 MHz [13]. To achieve larger bandwidths, a chirp train signal has to be generated. Since the phase values of the locked PLL are unknown, each subchirp has an unknown start phase.

Using this chirp train signal model, time delay estimation is more complicated. Dedicated algorithms are needed which require the full received signal. This can be problematic since the transmission speed is limited by the bus interface between the SDR and the host. In this chapter, an alternative to [13, 14] is presented.

This chapter focuses on the implementation details of a chirp compression algorithm which is implemented on an FPGA such that real-time processing for the required signal bandwidth is guaranteed.

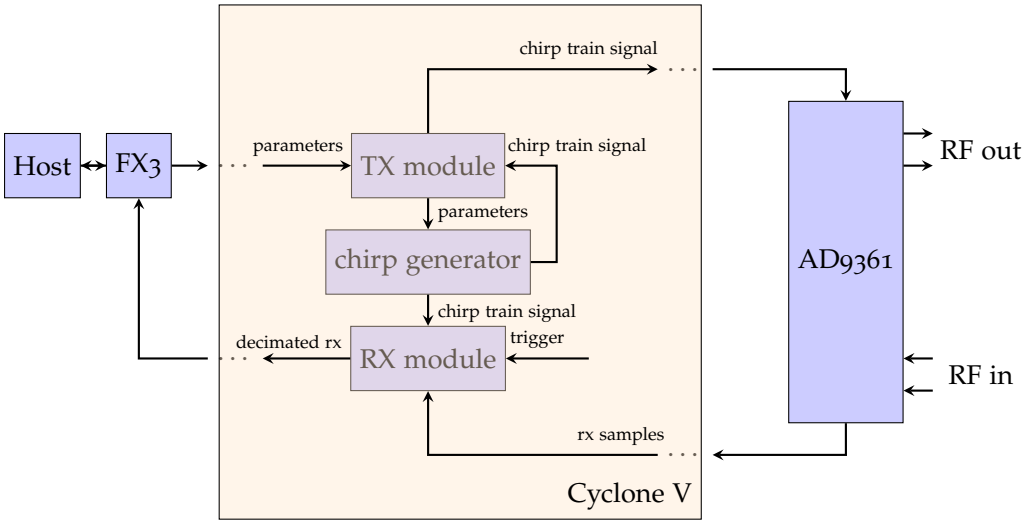

Figure 4.1: Gateware implementation where AD9361 is the RF transceiver and Cyclone V is the FPGA.

Figure 4.1 shows the FPGA implementation which is described in this chapter. It can be seen that the generated chirp-train signal is used inside the RX module. This is required for the downconversion of the received signal. Subsequently, the decimation takes place and the resulting bandwidth to the host is reduced. In addition, the chirp compression process is initiated by a trigger event, and rough synchronization is assumed. It is also possible to transmit the generated chirp-train signal.

4.2 Introduction to the SDR

The bladeRF 2.0 micro xA4 SDR is used for the implementation of the chirp compression algorithm. It supports a bandwidth of up to 61.44 MHz on each of the two transmitting and receiving channels at a quantization of 12 bit. The ISM band is covered as the frequency ranges from 47 MHz to 6 GHz. It should be noted that the bandwidth of the SDR already covers 77% of the required bandwidth of 80 MHz. For full coverage, the SDR needs to receive two times with different carrier frequencies.

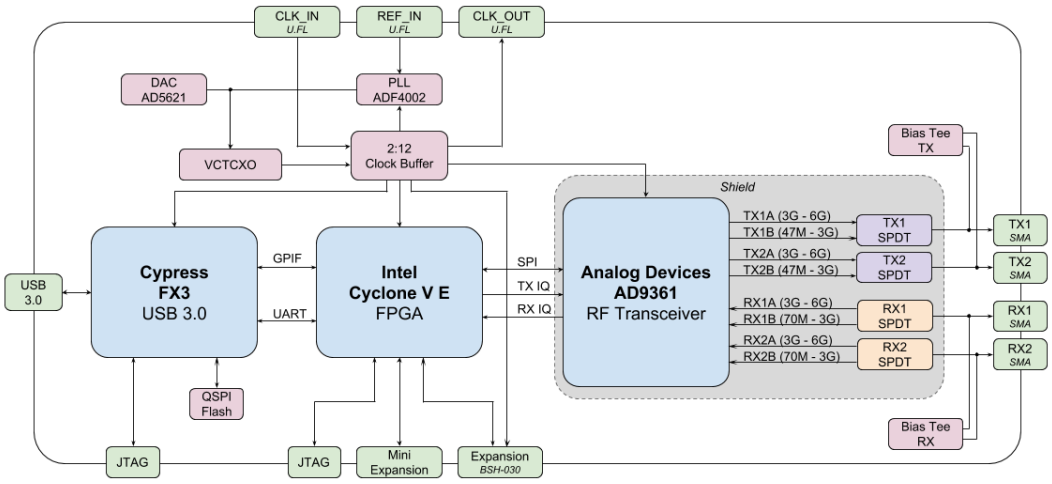

Figure 4.2: BladeRF 2.0 micro xA4 block diagram [15].

As shown in Figure 4.2, the received samples first pass the Analog Devices AD9361 transceiver and then are processed by an Altera Cyclone V FPGA. The processed samples are pushed onto a first in first out (FIFO) buffer. The same holds for the transmitted samples but in the reverse direction.

The Cypress FX3 processor is connected to the FIFO buffers using the GPIF interface. When samples are received using the libbladeRF library, the FX3 pops the samples from the FIFO buffer and sends them to the host over the Universal Serial Bus (USB) 3.0. Transmitted samples are first sent to the FX3 and then pushed onto the FIFO.

The USB 3.0 interface limits the transfer speed to about 400-500 MByte/s for raw data transfers [16]. When receiving at both channels and operating the SDR at the maximum sampling frequency of 61.44 MHz, the required transfer speed would already be at 491.52 MByte/s. Additional margins have to be considered since the raw data transfer rate of USB 3.0 has a strong variability depending on the devices and cables.

4.3 Chirp Train Parametrization

The chirp train signal generated with the CC2510 in [3] consists of multiple subchirps. In addition to the signal model from Equation (3.3b), each subchirp also consists of a pre-continuous wave (pre-CW) and a post-continuous wave (post-CW), which can be used to find the frequency offset error caused by the non-ideal PLL. The duration of the pre-CW, linear frequency chirp, post-CW, and pause is the same in each case. However, the start frequencies can be different. The amount of subchirps also has to be specified.

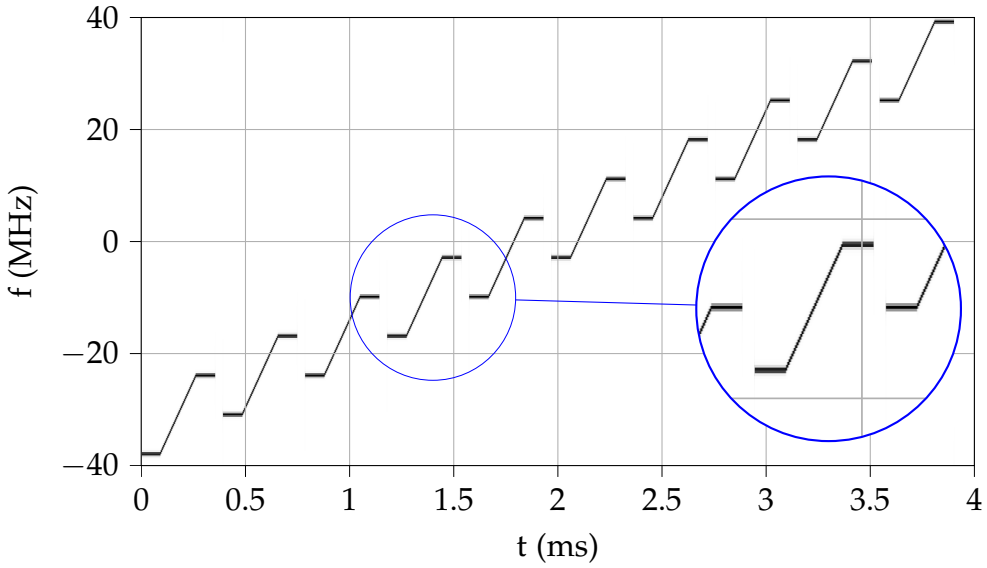

Figure 4.3: Example of a spectrogram of a baseband chirp train signal with additional pre-CW, post-CW, and pauses between the subchirps.

Each subchirp in Figure 4.3 consists of

- a pre-CW with an arbitrary start frequency,
- a linear frequency chirp with a fixed chirp rate and the start frequency of the pre-CW,
- a post-CW with a frequency corresponding to the end frequency of the linear frequency chirp and a
- a pause where the signal is zero.

4.4 Chirp Compression Algorithm

The goal of the chirp compression algorithm is to reduce the effective bandwidth of the signal. An intuitive approach to reducing the bandwidth is to multiply the signal, whose frequency is linearly increasing over time, with a carrier that is linearly decreasing. First of all, a time-delayed version of Equation (3.3b) is considered:

$$r(t) = x(t-\tau) = \exp(2\pi j\phi(t-\tau)) \tag{4.1a}$$

$$= \exp\left(2\pi j\left(\frac{k(t-\tau)^2}{2} + f_0(t-\tau)\right)\right) \tag{4.1b}$$

$$= x(t)\exp\left(2\pi j\left(\frac{k}{2}\left(\tau^2 - 2t\tau\right) - f_0\tau\right)\right). \tag{4.1c}$$

Sampling the received signal $r(t)$ leads to

$$r[n] = r(nT_s) = x[n]\exp\left(2\pi j\left(\frac{k}{2}\left(\tau^2 - 2nT_s\tau\right) - f_0\tau\right)\right) \tag{4.2a}$$

$$= r(nT_s) = x[n]\exp\left(2\pi j\left(\frac{m}{2T_s}\left(\tau^2 - 2nT_s\tau\right) - f_0\tau\right)\right). \tag{4.2b}$$

Multiplication with the complex conjugate of the sampled template chirp signal $x[n]$ results in

$$y[n] = r[n]x^*[n] \tag{4.3a}$$

$$= \exp\left(2\pi j\left(\frac{m}{2T_s}\left(\tau^2 - 2nT_s\tau\right) - f_0\tau\right)\right) \tag{4.3b}$$

$$= \exp(-2\pi jmn\tau)\exp\left(2\pi j\left(\frac{m}{2T_s}\tau^2 - f_0\tau\right)\right). \tag{4.3c}$$

The resulting signal of this downconversion is a complex sinusoidal signal consisting of a phase and a frequency that depend on the time delay and the chirp rate. This approach can be extended to a chirp train signal since its shape is also known by the receiver.

The downconversion process leads to a much smaller bandwidth of the signal. Therefore, the signal can be filtered and downsampled, which results in a reduced sampling rate at the host.

In summary, this means that the FPGA needs to generate the chirp train signal, multiply its conjugate with the received signal, and decimate the result to reduce the sampling rate.

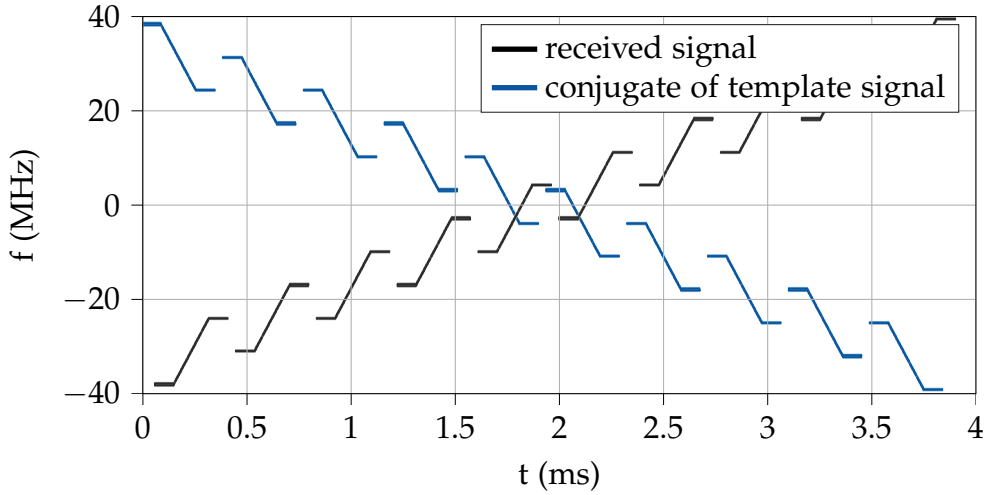

Figure 4.4: Example of a spectrogram of a received chirp train signal and the complex conjugate of the template signal.

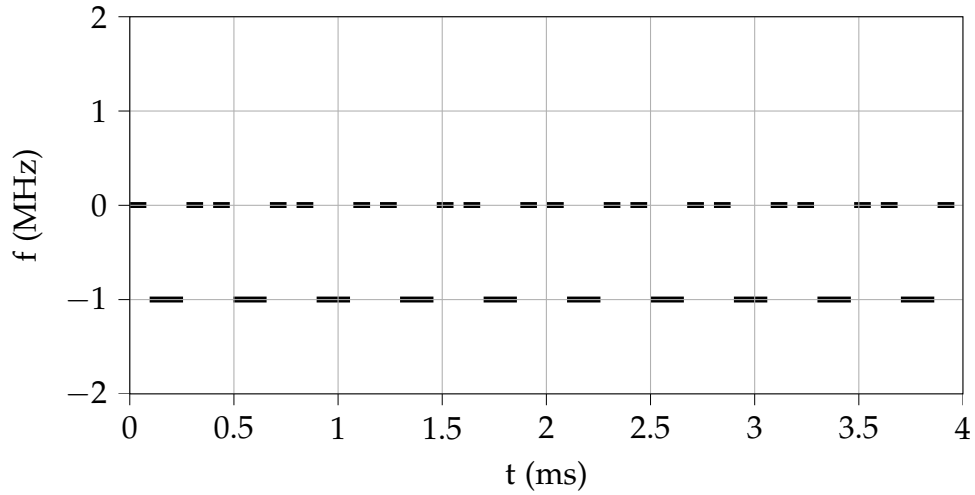

Figure 4.5: Spectrogram of a downconverted chirp train signal with $m = 1000$ Hz/s and $\tau = 1000T_s$ which leads to sinusoidal components with a frequency of -1 MHz.

Figure 4.4 shows the spectrogram of the complex conjugate of the chirp train signal and also a time-delayed version of the chirp train signal, which corresponds to the received signal. Figure 4.5 illustrates the time domain multiplication of these signals. It can be seen that the pre-CWs and the post-CWs are downconverted to 0 Hz since they do not have a frequency slope. The actual chirp components are downconverted to -1 MHz, allowing additional downsampling to reduce the sampling rate.

4.5 Gateware Implementation

The host configures the chirp train parameters and chooses the trigger event. After the trigger event, the chirp compression starts, and the decimated signal is sent to the host. The transmission of a chirp train signal is also possible in receive mode. Figure 4.1 illustrates the implementation.

4.5.1 Trigger Events

Chirp train generation and the chirp decimation process start when a trigger event occurs. The host selects one of the following trigger events:

- GPIO trigger: When a specific input pin is set to high.
- Power threshold trigger: When the instantaneous power is above a specific threshold for some time.
- Software trigger: The host sets a gateware register.

4.5.2 Fixed Point Numbers

The gateware does not support a floating point unit by default. An efficient alternative is to use fixed point numbers. Furthermore, the bladeRF already uses signed Q11 numbers for the I and Q samples, which is why this number representation is used. Another advantage of fixed point numbers is that multiplications and other arithmetic operations are efficient to compute since their implementation is the same as for integer operations.

4.5.3 Computation of the Chirp Train Signal

Direct Digital Synthesis (DDS) similar to [2] is used to compute the chirp signal. In this approach, the function values of the complex sinusoid are stored in a lookup table (LUT). Additionally, the phase which provides the input of the LUT needs to be calculated. A state machine is used to generate the chirp train signal including the pre-CW and post-CW.

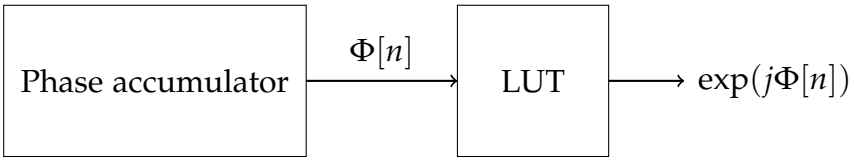

Figure 4.6: Computation of the chirp signal using DDS.

Lookup Table

For an efficient implementation, only a quarter period of a cosine function is stored in a table. The other part of the function is evaluated by negation and using the symmetric property of the function. Furthermore, the sine function is obtained by the phase shift property.

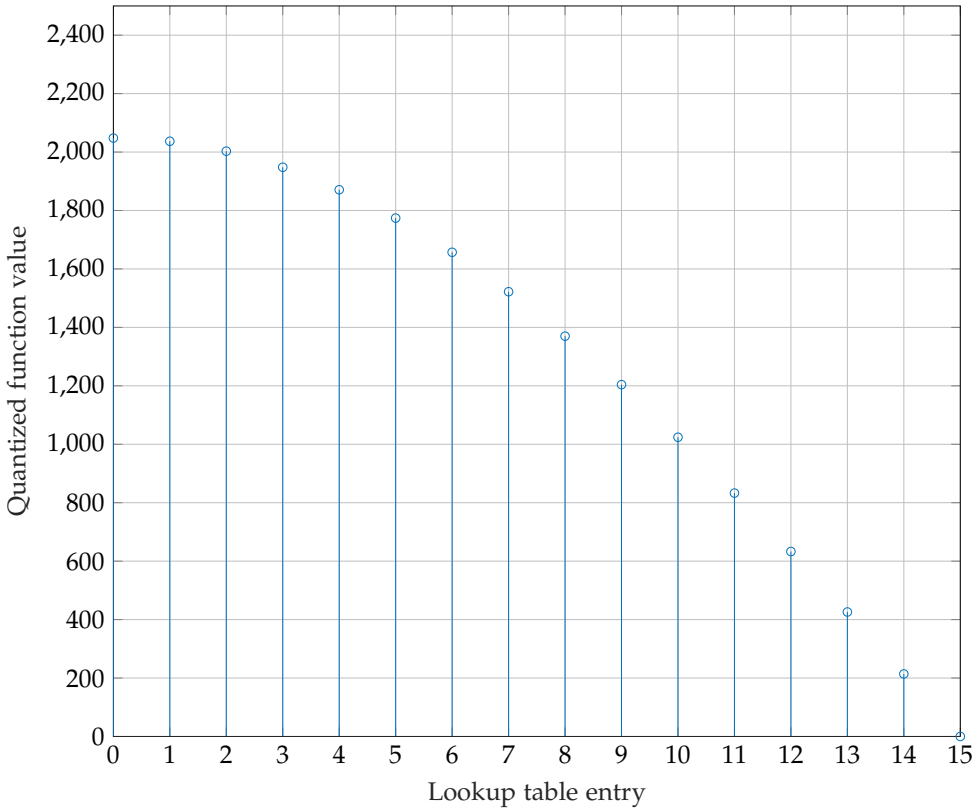

Figure 4.7: Example of a cosine LUT.

Figure 4.7 shows an example of a cosine LUT. The table length specifies the time resolution and the table entry size is the amplitude quantization of the cosine. The index of the table is obtained by normalizing the phase accumulator, multiplying it with the table size, and rounding it towards the closest integer.

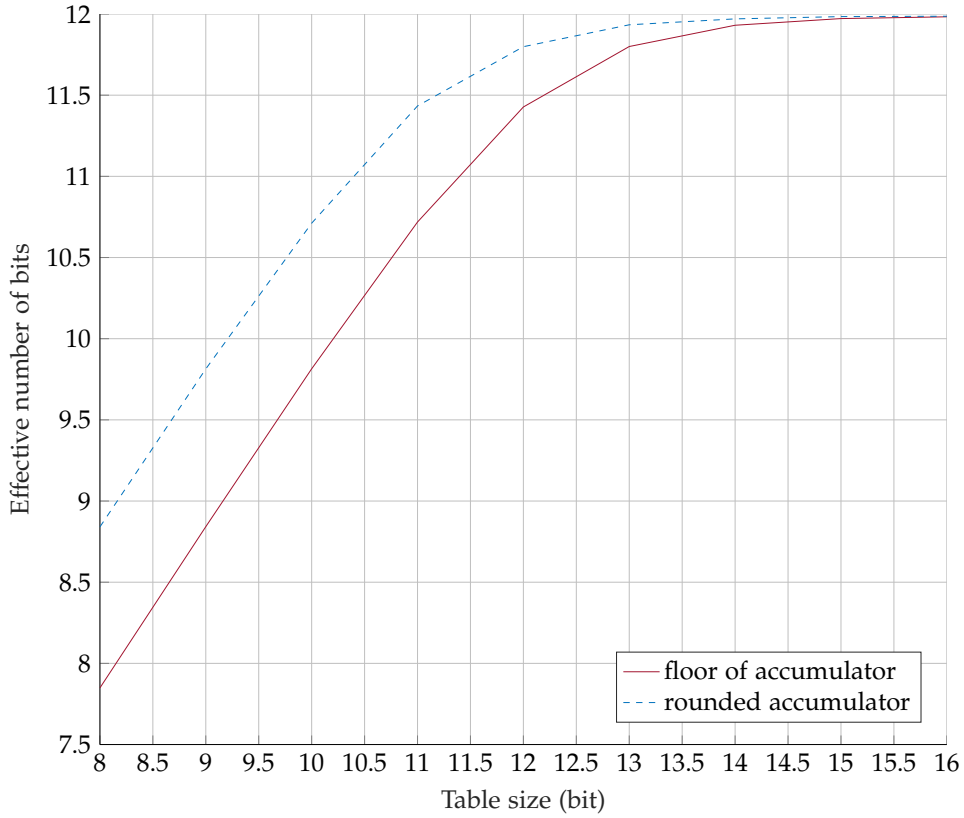

Figure 4.8: Effective number of bits for a cosine LUT.

From Figure 4.8 it can be observed that the table size has a large impact on the effective number of bits (ENOB) of the cosine. It can also be seen that rounding of the phase accumulator needs approximately one bit less in table size to achieve the same ENOB as for the floor case. To reach a good compromise of the LUT size and the ENOB in the gateware implementation, a table size of 12 bit is used together with a quantization of 12 bit and rounding.

Phase Calculation

It is possible to calculate the phase directly using single-cycle multiplication blocks, however, this approach is not resource-friendly. An efficient and accurate implementation of the phase calculation is achieved by trapezoidal integration as

$$\Phi[n] = \Phi_0 + 2\pi \int_0^{nT_s} f(t)dt \tag{4.4a}$$

$$= \Phi_0 + 2\pi \sum_{i=1}^{n} \frac{f[i] + f[i-1]}{2} T_s \tag{4.4b}$$

$$= \Phi[n-1] + 2\pi T_s \frac{f[n] + f[n-1]}{2} . \tag{4.4c}$$

A recursive relation for the phase can be obtained by

$$\Phi[n] = \Phi[n-1] + 2\pi T_s \frac{mn + f_0 + m(n-1) + f_0}{2} \tag{4.5a}$$

$$= \Phi[n-1] + 2\pi T_s \frac{mn + f_0 + m(n-1) + f_0}{2} \tag{4.5b}$$

$$= \Phi[n-1] + 2\pi T_s \frac{2mn + 2f_0 - m}{2} . \tag{4.5c}$$

This allows an efficient FPGA implementation since the current phase value depends on the previous one, a constant term, and an increment. The following Figure shows the gateware implementation and is based on [17].

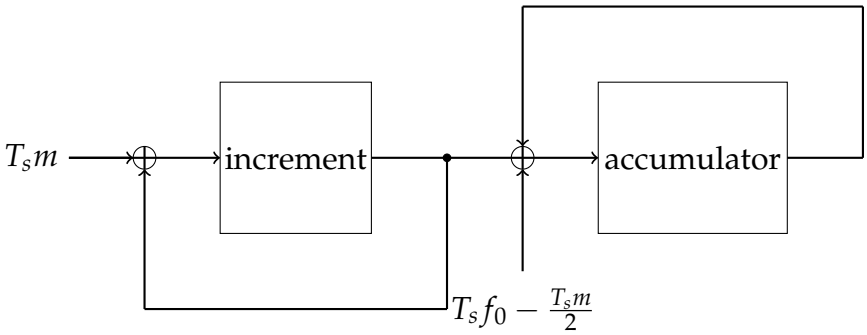

Figure 4.9: Computation of the phase for the chirp signal.

In Figure 4.9 a 2π normalized increment and accumulator register is used. To calculate the chirp signal, the output of the accumulator register is directly fed into the LUT. In the gateware implementation, the registers are defined as unsigned Q48 fixed point numbers. An overflow is possible and tolerated due to the 2π periodicity of the sinusoids.

4.5.4 Downconversion and Downsampling Stages

The downconversion is achieved by the multiplication of the received signal with the generated chirp train signal. The complex multiplication is implemented using additions and multiplications. The downconverted chirp train signal has to be filtered and downsampled to achieve a sampling rate reduction. Half-band filters are generated using the Intel Quartus Prime IP core generation tool. Each block decimates the signal by a factor of two. Higher decimation is achieved by cascading these decimation blocks. This process is done for both RX channels.

4.5.5 Communication with the Host

Chirp train parameters are stored in a config file at the host. These parameters need to be sent to the gateware. Since the usual transmission of signals from the host is not required, the values are injected into the TX data stream using a type–value scheme with fixed bit sizes. Internally, one sample consists of 24 bit, which means that larger values are split into smaller ones for the transmission. Chirp parameters are therefore stored in registers which are a multiple of 24 bit. After the configuration process, the host sends a flag to the gateware indicating that all parameters are set. When a trigger event occurs, a magic value including an internal timestamp is sent to the host indicating the start of the decimated signal. After the chirp decimation process is finished and the signal is sent to the host, a magic value indicating the end of the signal is appended to the RX data. This is possible for both RX channels.

Description	Name	Bit-size
Amount zero samples before chirp	T0	24
Amount pre-CW samples	T1	24
Amount actual chirp samples	T2	24
Amount post-CW samples	T3	24
Amount pause samples	TP	24
Chirp frequency increment	DF	48
Amount subchirps	AMOUNT_CHIRPS	24
List of start frequencies	FREQ_VEC	12x48

Table 4.1: Chirp parameter gateware registers

Table 4.1 shows the chirp parameters that are stored inside registers of the FPGA. Additional configuration parameters are:

- TRIGGER_MODE: Specifies the trigger mode (zero for GPIO trigger and one for the power threshold trigger).
- CHIRP_TX_ENABLED: Additionally transmit the chirp train signal after the trigger happens.
- DOWNSAMPLING_STAGE: Selects a downsampling stage (between 0 and 8). Each downsampling stage halves the sampling rate.
- CARRIER_FREQ: The carrier frequency of the SDR.
- RX_GAIN: The gain of the received signals.
- TX_GAIN: The gain of the transmitted signal.

5 Cramér–Rao Lower Bound for Time Delay Estimation

5.1 AWGN Case where only the Time Delay is Unknown

For the AWGN case from Equation (3.26), when the LOS channel coefficient and all start phases of the chirp-train signal are known, the unknown parameter is

$$\theta = \tau \, . \tag{5.1}$$

The time-delay error bound is given by [5] as

$$[\boldsymbol{\mathcal{I}}^{-1}(\boldsymbol{\theta})]_{11} = \frac{\sigma_w^2}{2|\alpha|^2 \|\dot{\boldsymbol{s}}\|^2} \tag{5.2}$$

$$= \frac{\sigma_w^2}{2|\alpha|^2 \|\dot{\boldsymbol{x}}\|^2} \, . \tag{5.3}$$

Equation (5.2) is simplified to Equation (5.3) using the vector norm simplification of the time derivative chirp train vector where

$$\|\dot{\boldsymbol{s}}\|^2 = \|\dot{\boldsymbol{x}}\|^2 \, , \tag{5.4}$$

which means that the signal energy of the time derivative chirp train vector is invariant of initial phase shifts of the chirp-train signal. It should also be noted that the same holds for the energy of the chirp train vector i.e.

$$\|\boldsymbol{s}\|^2 = \|\boldsymbol{x}\|^2 \, . \tag{5.5}$$

Similar to [6] the mean-square bandwidth is defined as

$$\beta^2 = \frac{\|\dot{\boldsymbol{x}}\|^2}{4\pi^2\|\boldsymbol{x}\|^2}\,, \tag{5.6}$$

and the signal-to-noise ratio is defined as

$$\mathrm{SNR} = \frac{|\alpha|^2\|\boldsymbol{x}\|^2}{\sigma_w^2}\,. \tag{5.7}$$

Using these definitions, the time-delay error bound from Equation (5.3) is rewritten as

$$[\boldsymbol{\mathcal{I}}^{-1}(\boldsymbol{\theta})]_{11} = \left(8\pi^2\beta^2\mathrm{SNR}\right)^{-1}\,. \tag{5.8}$$

Equation (5.8) shows that the CRLB is inversely proportional to the mean-square bandwidth β^2 and the SNR. It should be noted that if the sampling period T_s is small enough such that a sum is approximated by an integral, the mean-square bandwidth from Equation (5.6) can be written similar to [5] as

$$\beta^2 = \frac{T_s\|\dot{\boldsymbol{x}}\|^2}{T_s 4\pi^2\|\boldsymbol{x}\|^2} \tag{5.9a}$$

$$= \frac{\int_{-\infty}^{\infty} F^2|\bar{X}(F)|^2 dF}{\int_{-\infty}^{\infty}|\bar{X}(F)|^2 dF} \tag{5.9b}$$

$$= \frac{\int_{-fs/2}^{fs/2} F^2|\bar{X}(F)|^2 dF}{\int_{-fs/2}^{fs/2}|\bar{X}(F)|^2 dF}\,, \tag{5.9c}$$

where $\bar{X}(F)$ is the Fourier transform of the chirp-train signal in the time domain for a frequency F. The simplification from Equation (5.9b) to Equation (5.9c) is possible since the chirp-train signal is band-limited between $-f_s/2$ and $f_s/2$.

5.2 AWGN Case where only the first Phase is Unknown

The signal model from Equation (3.26) is used and it is assumed that the initial phases of the chirp-train signal are known. Hence, the phase vector $\boldsymbol{p}$ is treated to be known. The estimation parameters are shown in the parameter vector

$$\boldsymbol{\theta} = [\tau, |\alpha|, \arg(\alpha)]^T \ . \tag{5.10}$$

Using the mean of Equation (3.26) with

$$\boldsymbol{\mu}(\boldsymbol{\theta}) = \alpha \boldsymbol{W}^H \boldsymbol{P}(\tau) \boldsymbol{W} \boldsymbol{X} \boldsymbol{p} \in \mathbb{C}^M \ , \tag{5.11}$$

the FIM entry for the time delay τ is calculated using Equation (2.6):

$$[\boldsymbol{\mathcal{I}}(\boldsymbol{\theta})]_{11} = \frac{2}{\sigma_w^2} \mathrm{Re}\left\{ \left(\frac{\partial \boldsymbol{\mu}(\boldsymbol{\theta})}{\partial \tau} \right)^H \frac{\partial \boldsymbol{\mu}(\boldsymbol{\theta})}{\partial \tau} \right\} \tag{5.12a}$$

$$= \frac{2}{\sigma_w^2} \mathrm{Re}\left\{ |\alpha|^2 \boldsymbol{s}^H \boldsymbol{W}^H \boldsymbol{D}^2 \boldsymbol{W} \boldsymbol{s} \right\} \tag{5.12b}$$

$$= \frac{2|\alpha|^2}{\sigma_w^2} \|\boldsymbol{D}\boldsymbol{W}\boldsymbol{s}\|^2 \tag{5.12c}$$

$$= \frac{2|\alpha|^2}{\sigma_w^2} \|\boldsymbol{W}^H \boldsymbol{D}\boldsymbol{W}\boldsymbol{s}\|^2 \tag{5.12d}$$

$$= \frac{2|\alpha|^2}{\sigma_w^2} \|\dot{\boldsymbol{s}}\|^2 \ , \tag{5.12e}$$

where

$$\boldsymbol{D} = \frac{2\pi j f_s}{M} \mathrm{diag}\left(\left[-\frac{M}{2}, \ldots, \frac{M}{2} - 1 \right] \right) \ , \tag{5.13}$$

is the frequency domain time derivative matrix for the sampling frequency f_s. Therefore, Equation (5.12d) can be written as

$$\dot{\boldsymbol{s}} = \boldsymbol{W}^H \boldsymbol{D} \boldsymbol{W} \boldsymbol{s} \ , \tag{5.14}$$

where $\dot{\boldsymbol{s}}$ is the time domain derivative vector of the chirp-train signal according to Equation (3.17). In Equation (5.12e) it can be seen that the information for the time delay τ is proportional to the energy of the time derivative chirp-train signal. Moreover, Equation (5.12c) has a similar form as the numerator from Equation (5.9c). These terms are in fact the same, except of a scaling factor if T_s is small enough. This is evident as Equation (5.12e) can be rewritten as a scaled version of the numerator of Equation (5.9c).

For the magnitude $|\alpha|$ of the LOS channel coefficient the FIM entry evaluates to

$$[\boldsymbol{\mathcal{I}}(\boldsymbol{\theta})]_{22} = \frac{2}{\sigma_w^2} \operatorname{Re}\left\{ \left(\frac{\partial \boldsymbol{\mu}(\boldsymbol{\theta})}{\partial |\alpha|} \right)^H \frac{\partial \boldsymbol{\mu}(\boldsymbol{\theta})}{\partial |\alpha|} \right\} \tag{5.15a}$$

$$= \frac{2}{\sigma_w^2} \|\boldsymbol{s}\|^2 , \tag{5.15b}$$

where $\|\boldsymbol{s}\|^2$ corresponds to the signal energy of the chirp-train signal. The FIM entry for the phase $\arg(\alpha)$ of the LOS channel coefficient is

$$[\boldsymbol{\mathcal{I}}(\boldsymbol{\theta})]_{33} = \frac{2}{\sigma_w^2} \operatorname{Re}\left\{ \left(\frac{\partial \boldsymbol{\mu}(\boldsymbol{\theta})}{\partial \arg(\alpha)} \right)^H \frac{\partial \boldsymbol{\mu}(\boldsymbol{\theta})}{\partial \arg(\alpha)} \right\} \tag{5.16a}$$

$$= \frac{2|\alpha|^2}{\sigma_w^2} \|\boldsymbol{s}\|^2 . \tag{5.16b}$$

Equations (5.15b) and (5.16b) show that the information for the magnitude and the phase of the LOS channel coefficient is proportional to the signal energy of the chirp train. For the time delay τ and the magnitude $|\alpha|$ of the LOS channel coefficient the corresponding FIM entry evaluates to

$$[\boldsymbol{\mathcal{I}}(\boldsymbol{\theta})]_{12} = \frac{2}{\sigma_w^2} \operatorname{Re}\left\{ \left(\frac{\partial \boldsymbol{\mu}(\boldsymbol{\theta})}{\partial \tau} \right)^H \frac{\partial \boldsymbol{\mu}(\boldsymbol{\theta})}{\partial |\alpha|} \right\} \tag{5.17a}$$

$$= -\frac{2|\alpha|}{\sigma_w^2} \operatorname{Re}\left\{ \boldsymbol{s}^H \boldsymbol{W}^H \boldsymbol{D} \boldsymbol{W} \boldsymbol{s} \right\} \tag{5.17b}$$

$$= -\frac{2|\alpha|}{\sigma_w^2} \operatorname{Re}\left\{ \boldsymbol{s}^H \dot{\boldsymbol{s}} \right\} . \tag{5.17c}$$

The simplification from Equation (5.17b) to Equation (5.17c) is possible using the time derivative property from Equation (5.14). For the time delay τ and the phase $\arg(\alpha)$ of the LOS channel coefficient the corresponding FIM entry is calculated as

$$[\boldsymbol{\mathcal{I}}(\boldsymbol{\theta})]_{13} = \frac{2}{\sigma_w^2} \mathrm{Re}\left\{ \left(\frac{\partial \boldsymbol{\mu}(\boldsymbol{\theta})}{\partial \tau} \right)^H \frac{\partial \boldsymbol{\mu}(\boldsymbol{\theta})}{\partial \arg(\alpha)} \right\} \tag{5.18a}$$

$$= -\frac{2|\alpha|^2}{\sigma_w^2} \mathrm{Re}\left\{ j\boldsymbol{s}^H \boldsymbol{W}^H \boldsymbol{D} \boldsymbol{W} \boldsymbol{s} \right\} \tag{5.18b}$$

$$= \frac{2|\alpha|^2}{\sigma_w^2} \mathrm{Im}\left\{ \boldsymbol{s}^H \dot{\boldsymbol{s}} \right\} . \tag{5.18c}$$

The time derivative property from Equation (5.14) is again used for simplifying Equation (5.18b) to Equation (5.18c). The FIM entry for the magnitude $|\alpha|$ and the phase $\arg(\alpha)$ of the LOS channel coefficient evaluates to

$$[\boldsymbol{\mathcal{I}}(\boldsymbol{\theta})]_{23} = \frac{2}{\sigma_w^2} \mathrm{Re}\left\{ \left(\frac{\partial \boldsymbol{\mu}(\boldsymbol{\theta})}{\partial |\alpha|} \right)^H \frac{\partial \boldsymbol{\mu}(\boldsymbol{\theta})}{\partial \arg(\alpha)} \right\} \tag{5.19a}$$

$$= \frac{2|\alpha|}{\sigma_w^2} \mathrm{Re}\left\{ j\boldsymbol{s}^H \boldsymbol{s} \right\} \tag{5.19b}$$

$$= 0 . \tag{5.19c}$$

The time-delay error bound is the bound of interest and therefore, the element in the first column and first row of the inverse FIM has to be calculated. Similar to [12] this can be achieved by writing the FIM in the form

$$\boldsymbol{\mathcal{I}}(\boldsymbol{\theta}) = \frac{2}{\sigma_w^2} \begin{bmatrix} F & \boldsymbol{G} \\ \boldsymbol{G}^T & \boldsymbol{H} \end{bmatrix} , \tag{5.20}$$

and computing the corresponding matrix element of the inverse FIM using the Schur complement as

$$[\boldsymbol{\mathcal{I}}^{-1}(\boldsymbol{\theta})]_{11} = \frac{\sigma_w^2}{2} (F - \boldsymbol{G}\boldsymbol{H}^{-1}\boldsymbol{G}^T)^{-1} . \tag{5.21}$$

The scalar $F \in \mathbb{R}$ and the row vector $\boldsymbol{G} \in \mathbb{R}^{1\times 2}$ can be obtained by structuring the FIM entries as

$$F = |\alpha|^2 \|\dot{\boldsymbol{s}}\|^2 \,, \tag{5.22}$$

$$\boldsymbol{G} = \left[-|\alpha| \operatorname{Re}\left\{ \boldsymbol{s}^H \dot{\boldsymbol{s}} \right\}, |\alpha|^2 \operatorname{Im}\left\{ \boldsymbol{s}^H \dot{\boldsymbol{s}} \right\} \right] \,, \tag{5.23}$$

The matrix $\boldsymbol{H} \in \mathbb{R}^{2\times 2}$ is written as

$$\boldsymbol{H} = \|s\|^2 \begin{bmatrix} 1 & 0 \\ 0 & |\alpha|^2 \end{bmatrix} \,. \tag{5.24}$$

Therefore, the time-delay error bound from Equation (5.21) can be written as

$$[\boldsymbol{\mathcal{I}}^{-1}(\boldsymbol{\theta})]_{11} = \frac{\sigma_w^2}{2} \left(|\alpha|^2 \|\dot{\boldsymbol{s}}\|^2 - \frac{|\alpha|^2}{\|s\|^2} \operatorname{Re}\left\{ \boldsymbol{s}^H \dot{\boldsymbol{s}} \right\}^2 - \frac{|\alpha|^2}{\|s\|^2} \operatorname{Im}\left\{ \boldsymbol{s}^H \dot{\boldsymbol{s}} \right\}^2 \right)^{-1} \tag{5.25a}$$

$$= \frac{\sigma_w^2}{2|\alpha|^2} \left(\|\dot{\boldsymbol{s}}\|^2 - \frac{|\boldsymbol{s}^H \dot{\boldsymbol{s}}|^2}{\|\boldsymbol{s}\|^2} \right)^{-1} \tag{5.25b}$$

$$= \frac{\sigma_w^2}{2|\alpha|^2} \left(\|\dot{\boldsymbol{x}}\|^2 - \frac{\operatorname{Im}\{\boldsymbol{x}^H \dot{\boldsymbol{x}}\}^2}{\|\boldsymbol{x}\|^2} \right)^{-1} \,. \tag{5.25c}$$

Equation (5.25b) simplifies to Equation (5.25c) since the vector norms do not depend on the phase shifts as it can be seen in Equation (5.4). Another simplification was made using Equation (3.16b) where

$$|\boldsymbol{x}^H \dot{\boldsymbol{x}}|^2 = \operatorname{Im}\left\{ \boldsymbol{x}^H \dot{\boldsymbol{x}} \right\}^2 \,. \tag{5.26}$$

Using the definition of the mean-square bandwidth β^2 from Equation (5.6) and an additional definition of the signal-to-interference-plus-noise ratio which in this case is defined as

$$\mathrm{SINR}_\mathrm{I} = \frac{|\alpha|^2 \left(\|\boldsymbol{x}\|^2 - \operatorname{Im}\{\boldsymbol{x}^H \dot{\boldsymbol{x}}\}^2 / \|\dot{\boldsymbol{x}}\|^2 \right)}{\sigma_w^2} \,, \tag{5.27}$$

Equation (5.25c) can be written as

$$[\boldsymbol{\mathcal{I}}^{-1}(\boldsymbol{\theta})]_{11} = \left(8\pi^2\beta^2\mathrm{SINR}_{\mathrm{I}}\right)^{-1} . \tag{5.28}$$

In contrast to the time-delay error bound from Equation (5.28), where all phases are known, the time-delay error bound for this case is reduced. This happens because of the subtractive term in Equation (5.27). The term describes the diminished information caused by the phase estimation.

An alternative representation of the time-delay error bound is found by using the SNR instead of $\mathrm{SINR}_{\mathrm{I}}$, but including the information loss of the additional estimation parameters in the root-mean-square (RMS) bandwidth. This can be seen in Appendix A in Equation (A.7d) where the time-delay error bound is given as

$$[\boldsymbol{\mathcal{I}}^{-1}(\boldsymbol{\theta})]_{11} = \left(8\pi^2\ \mathrm{SNR}\ \tilde{\beta}^2\right)^{-1} . \tag{5.29}$$

It can be seen from Equation (A.12f), that the reduced RMS bandwidth $\tilde{\beta}$ for a chirp signal is the same as the RMS bandwidth β for the case of a frequency-symmetric chirp signal. Furthermore, for the case of a frequency-symmetric chirp, the RMS bandwidth reduction is zero since the information-loss term vanishes, as seen in Equation (A.2c).

5.3 AWGN Case where all Phases are Unknown

The signal model from Equation (3.28) is used where the mean is written as

$$\boldsymbol{\mu}(\boldsymbol{\theta}) = |\alpha|\boldsymbol{W}^H\boldsymbol{P}(\tau)\boldsymbol{W}\boldsymbol{X}\boldsymbol{p} \in \mathbb{C}^M , \tag{5.30}$$

and the parameter vector is defined as

$$\boldsymbol{\theta} = [\tau, |\alpha|, \phi]^T . \tag{5.31}$$

In this case, the individual phases of the chirp-train signal model are unknown. The FIM element for the time delay τ is similar to Equation (5.12e) and written as

$$[\boldsymbol{\mathcal{I}}(\boldsymbol{\theta})]_{11} = \frac{2}{\sigma_w^2} \mathrm{Re}\left\{ \left(\frac{\partial \boldsymbol{\mu}(\boldsymbol{\theta})}{\partial \tau} \right)^H \frac{\partial \boldsymbol{\mu}(\boldsymbol{\theta})}{\partial \tau} \right\} \tag{5.32a}$$

$$= \frac{2|\alpha|^2}{\sigma_w^2} \|\dot{\boldsymbol{s}}\|^2 \,. \tag{5.32b}$$

It can be seen that the whole derivative chirp train contains information about the time delay τ. For the magnitude $|\alpha|$ of the LOS channel coefficient the FIM entry evaluates to

$$[\boldsymbol{\mathcal{I}}(\boldsymbol{\theta})]_{22} = \frac{2}{\sigma_w^2} \mathrm{Re}\left\{ \left(\frac{\partial \boldsymbol{\mu}(\boldsymbol{\theta})}{\partial |\alpha|} \right)^H \frac{\partial \boldsymbol{\mu}(\boldsymbol{\theta})}{\partial |\alpha|} \right\} \tag{5.33a}$$

$$= \frac{2}{\sigma_w^2} \|\boldsymbol{s}\|^2 \,, \tag{5.33b}$$

$$\tag{5.33c}$$

which means that the information for the magnitude is proportional to the energy of the whole chirp-train signal. For the phases ϕ of the chirp-train signal the corresponding FIM element evaluates to

$$[\boldsymbol{\mathcal{I}}(\boldsymbol{\theta})]_{33} = \frac{2}{\sigma_w^2} \mathrm{Re}\left\{ \left(\frac{\partial \boldsymbol{\mu}(\boldsymbol{\theta})}{\partial \boldsymbol{\phi}} \right)^H \frac{\partial \boldsymbol{\mu}(\boldsymbol{\theta})}{\partial \boldsymbol{\phi}} \right\} \tag{5.34a}$$

$$= \frac{2|\alpha|^2}{\sigma_w^2} \mathrm{Re}\Big\{ \mathrm{diag}(\boldsymbol{p})^H \boldsymbol{X}^H \boldsymbol{X}\, \mathrm{diag}(\boldsymbol{p}) \Big\} \tag{5.34b}$$

$$= \frac{2|\alpha|^2}{\sigma_w^2} \mathrm{Re}\Big\{ \boldsymbol{S}^H \boldsymbol{S} \Big\} \,. \tag{5.34c}$$

Equation (5.34b) is simplified to Equation (5.34c) using the matrix $\boldsymbol{S}$ from Equation (3.13) which contains the phase-shifted chirps in each column. It can be seen that information for the i-th phase is contained in the i-th subchirp only. The FIM element for the time delay $\boldsymbol{\tau}$ and the magnitude $|\alpha|$

of the LOS channel coefficient is calculated as

$$[\boldsymbol{\mathcal{I}}(\boldsymbol{\theta})]_{12} = \frac{2}{\sigma_w^2}\,\mathrm{Re}\left\{\left(\frac{\partial\boldsymbol{\mu}(\boldsymbol{\theta})}{\partial\tau}\right)^H \frac{\partial\boldsymbol{\mu}(\boldsymbol{\theta})}{\partial|\alpha|}\right\} \tag{5.35a}$$

$$= -\frac{2|\alpha|}{\sigma_w^2}\,\mathrm{Re}\Big\{\boldsymbol{p}^H\boldsymbol{X}^H\boldsymbol{W}^H\boldsymbol{D}\boldsymbol{W}\boldsymbol{X}\boldsymbol{p}\Big\} \tag{5.35b}$$

$$= -\frac{2|\alpha|}{\sigma_w^2}\,\mathrm{Re}\Big\{\boldsymbol{s}^H\dot{\boldsymbol{s}}\Big\}\,. \tag{5.35c}$$

Equation (5.35b) simplifies to Equation (5.35c) using the identity from Equation (5.14). For the time delay $\boldsymbol{\tau}$ and the phases $\boldsymbol{\phi}$ of the chirp train-signal model, the corresponding FIM element calculates to

$$[\boldsymbol{\mathcal{I}}(\boldsymbol{\theta})]_{13} = \frac{2}{\sigma_w^2}\,\mathrm{Re}\left\{\left(\frac{\partial\boldsymbol{\mu}(\boldsymbol{\theta})}{\partial\tau}\right)^H \frac{\partial\boldsymbol{\mu}(\boldsymbol{\theta})}{\partial\boldsymbol{\phi}}\right\} \tag{5.36a}$$

$$= -\frac{2|\alpha|^2}{\sigma_w^2}\,\mathrm{Re}\Big\{j\boldsymbol{p}^H\boldsymbol{X}^H\boldsymbol{W}^H\boldsymbol{D}\boldsymbol{W}\boldsymbol{X}\,\mathrm{diag}(\boldsymbol{p})\Big\} \tag{5.36b}$$

$$= -\frac{2|\alpha|^2}{\sigma_w^2}\,\mathrm{Re}\Big\{j\boldsymbol{p}^H\boldsymbol{X}^H\boldsymbol{W}^H\boldsymbol{D}\boldsymbol{W}\boldsymbol{S}\Big\} \tag{5.36c}$$

$$= \frac{2|\alpha|^2}{\sigma_w^2}\,\mathrm{Im}\Big\{\boldsymbol{s}^H\dot{\boldsymbol{S}}\Big\}\,. \tag{5.36d}$$

Equation (5.36c) simplifies to Equation (5.36d) due to

$$\dot{\boldsymbol{S}} = \boldsymbol{W}^H\boldsymbol{D}\boldsymbol{W}\boldsymbol{S}\,, \tag{5.37}$$

where the matrix $\dot{\boldsymbol{S}}$, which is defined in Equation (3.21) contains the time derivatives of the phase-shifted chirps in each column. For the magnitude $|\alpha|$ of the LOS channel coefficient and the phases $\boldsymbol{\phi}$ of the chirp-train signal model the FIM entry is calculated as

$$[\boldsymbol{\mathcal{I}}(\boldsymbol{\theta})]_{23} = \frac{2}{\sigma_w^2}\,\mathrm{Re}\left\{\left(\frac{\partial\boldsymbol{\mu}(\boldsymbol{\theta})}{\partial|\alpha|}\right)^H \frac{\partial\boldsymbol{\mu}(\boldsymbol{\theta})}{\partial\boldsymbol{\phi}}\right\} \tag{5.38a}$$

$$= \frac{2|\alpha|}{\sigma_w^2}\,\mathrm{Re}\Big\{j\boldsymbol{p}^H\boldsymbol{X}^H\boldsymbol{X}\,\mathrm{diag}(\boldsymbol{p})\Big\} \tag{5.38b}$$

$$= -\frac{2|\alpha|}{\sigma_w^2}\,\mathrm{Im}\Big\{\boldsymbol{s}^H\boldsymbol{S}\Big\}\,. \tag{5.38c}$$

The FIM is again written in the form of Equation (5.20) with

$$F = |\alpha|^2 \|\dot{\boldsymbol{s}}\|^2 \in \mathbb{R}, \tag{5.39}$$

$$\boldsymbol{G} = \left[-|\alpha| \operatorname{Re}\left\{ \boldsymbol{s}^H \dot{\boldsymbol{s}} \right\}, |\alpha|^2 \operatorname{Im}\left\{ \boldsymbol{s}^H \dot{\boldsymbol{S}} \right\} \right] \in \mathbb{R}^{1 \times (P+1)} , \tag{5.40}$$

and

$$\boldsymbol{H} = \begin{bmatrix} \|\boldsymbol{s}\|^2 & -|\alpha| \operatorname{Im}\{\boldsymbol{s}^H \boldsymbol{S}\} \\ -|\alpha| \operatorname{Im}\{\boldsymbol{s}^H \boldsymbol{S}\}^T & |\alpha|^2 \operatorname{Re}\{\boldsymbol{S}^H \boldsymbol{S}\} \end{bmatrix} \in \mathbb{R}^{(P+1)\times(P+1)} . \tag{5.41}$$

The time delay bound is again calculated as

$$[\boldsymbol{\mathcal{I}}^{-1}(\boldsymbol{\theta})]_{11} = \frac{\sigma_w^2}{2} (F - \boldsymbol{G}\boldsymbol{H}^{-1}\boldsymbol{G}^T)^{-1} \tag{5.42a}$$

$$= \frac{\sigma_w^2}{2} (|\alpha|^2 \|\dot{\boldsymbol{s}}\|^2 - \boldsymbol{G}\boldsymbol{H}^{-1}\boldsymbol{G}^T)^{-1} , \tag{5.42b}$$

where

$$\boldsymbol{G}\boldsymbol{H}^{-1}\boldsymbol{G}^T = \begin{bmatrix} -|\alpha| \operatorname{Re}\{\boldsymbol{s}^H \dot{\boldsymbol{s}}\} \\ |\alpha|^2 \operatorname{Im}\{\boldsymbol{s}^H \dot{\boldsymbol{S}}\} \end{bmatrix}^T \begin{bmatrix} \|\boldsymbol{s}\|^2 & -a \operatorname{Im}\{\boldsymbol{s}^H \boldsymbol{S}\} \\ -|\alpha| \operatorname{Im}\{\boldsymbol{s}^H \boldsymbol{S}\}^T & |\alpha|^2 \operatorname{Re}\{\boldsymbol{S}^H \boldsymbol{S}\} \end{bmatrix}^{-1} \begin{bmatrix} -|\alpha| \operatorname{Re}\{\boldsymbol{s}^H \dot{\boldsymbol{s}}\} \\ |\alpha|^2 \operatorname{Im}\{\boldsymbol{s}^H \dot{\boldsymbol{S}}\} \end{bmatrix} . \tag{5.43}$$

Using the property

$$\operatorname{Im}\left\{ \boldsymbol{s}^H \boldsymbol{S} \right\} = 0 , \tag{5.44}$$

Equation (5.43) simplifies to

$$\boldsymbol{G}\boldsymbol{H}^{-1}\boldsymbol{G}^T = \begin{bmatrix} -|\alpha| \operatorname{Re}\{\boldsymbol{s}^H \dot{\boldsymbol{s}}\} \\ |\alpha|^2 \operatorname{Im}\{\boldsymbol{s}^H \dot{\boldsymbol{S}}\} \end{bmatrix}^T \begin{bmatrix} \|\boldsymbol{s}\|^2 & 0 \\ 0 & |\alpha|^2 \operatorname{Re}\{\boldsymbol{S}^H \boldsymbol{S}\} \end{bmatrix}^{-1} \begin{bmatrix} -|\alpha| \boldsymbol{s}^H \dot{\boldsymbol{s}} \\ |\alpha|^2 \operatorname{Im}\{\boldsymbol{s}^H \dot{\boldsymbol{S}}\} \end{bmatrix} \tag{5.45a}$$

$$= |\alpha|^2 \operatorname{Re}\left\{ \boldsymbol{s}^H \dot{\boldsymbol{s}} \right\}^2 + |\alpha|^2 \operatorname{Im}\left\{ \boldsymbol{s}^H \dot{\boldsymbol{S}} \right\} \operatorname{Re}\left\{ \boldsymbol{S}^H \boldsymbol{S} \right\} \operatorname{Im}\left\{ \boldsymbol{s}^H \dot{\boldsymbol{S}} \right\}^T . \tag{5.45b}$$

Due to the property from Equation (3.16b) it can be seen that the multiplication of the chirp train with the time derivative of the chirp train is imaginary i.e.

$$\mathrm{Re}\left\{\boldsymbol{s}^H\dot{\boldsymbol{s}}\right\}^2 = 0\,. \tag{5.46}$$

Since the columns of the chirp train matrix $\boldsymbol{S}$ are orthogonal with

$$\mathrm{Re}\left\{\boldsymbol{S}^H\boldsymbol{S}\right\} = \mathrm{diag}\left(\left[\|\boldsymbol{s}_i\|^2\right]_{i=0}^{P-1}\right)\,, \tag{5.47}$$

and due to

$$\begin{aligned}\mathrm{Im}\left\{\boldsymbol{s}^H\dot{\boldsymbol{S}}\right\} &= \mathrm{Im}\left\{\boldsymbol{p}^H\boldsymbol{X}^H\dot{\boldsymbol{X}}\,\mathrm{diag}(\boldsymbol{p})\right\} &(5.48)\\ &= \left[\mathrm{Im}\left\{\boldsymbol{s}_0^H\dot{\boldsymbol{s}}_0\right\},\ldots,\mathrm{Im}\left\{\boldsymbol{s}_{P-1}^H\dot{\boldsymbol{s}}_{P-1}\right\}\right]\,, &(5.49)\end{aligned}$$

Equation (5.45b) simplifies to

$$\boldsymbol{G}\boldsymbol{H}^{-1}\boldsymbol{G}^T = |\alpha|^2\sum_{i=0}^{P-1}\frac{\mathrm{Im}\{\boldsymbol{s}_i^H\dot{\boldsymbol{s}}_i\}^2}{\|\boldsymbol{s}_i\|^2}\,. \tag{5.50}$$

Inserting Equation (5.50) into Equation (5.42b) leads to

$$\begin{aligned}[\boldsymbol{\mathcal{I}}^{-1}(\boldsymbol{\theta})]_{11} &= \frac{\sigma_w^2}{2|\alpha|^2}\left(\|\dot{\boldsymbol{s}}\|^2 - \sum_{i=0}^{P-1}\frac{\mathrm{Im}\{\boldsymbol{s}_i^H\dot{\boldsymbol{s}}_i\}^2}{\|\boldsymbol{s}_i\|^2}\right)^{-1} &(5.51a)\\ &= \frac{\sigma_w^2}{2|\alpha|^2}\left(\|\dot{\boldsymbol{x}}\|^2 - \sum_{i=0}^{P-1}\frac{\mathrm{Im}\{\boldsymbol{x}_i^H\dot{\boldsymbol{x}}_i\}^2}{\|\boldsymbol{x}_i\|^2}\right)^{-1}\,. &(5.51b)\end{aligned}$$

The definition of the mean-square bandwidth β^2 from Equation (5.6) is used again. The SINR in this case calculates to

$$\mathrm{SINR}_{\mathrm{II}} = \frac{|\alpha|^2}{\sigma_w^2}\left(\|\boldsymbol{x}\|^2 - \frac{\|\boldsymbol{x}\|^2}{\|\dot{\boldsymbol{x}}\|^2}\sum_{i=0}^{P-1}\frac{\mathrm{Im}\{\boldsymbol{x}_i^H\dot{\boldsymbol{x}}_i\}^2}{\|\boldsymbol{x}_i\|^2}\right)\,. \tag{5.52}$$

Therefore, Equation (5.51b) can be written as

$$[\boldsymbol{\mathcal{I}}^{-1}(\boldsymbol{\theta})]_{11} = \left(8\pi^2\beta^2\mathrm{SINR}_{\mathrm{II}}\right)^{-1}\,. \tag{5.53}$$

The SINR from Equation (5.52) which considers that all phases of the chirp train are unknown, is different from the SINR from Equation (5.27) when only the initial phase is unknown. This happens due to the additional phase estimation parameters.

In Appendix A, the time-delay error bound from Equation (5.51b) is simplified for a chirp-train signal which is given as

$$[\boldsymbol{\mathcal{I}}^{-1}(\boldsymbol{\theta})]_{11} = \frac{12P^2}{8\pi^2 \,\mathrm{SNR}\, B^2}\,, \tag{5.54}$$

where $B = mN$ is the absolute bandwidth a single chirp of length N and the linear chirp rate m would achieve. It can be seen that the result is independent of the start frequencies of the individual subchirps. Furthermore, increasing the length of the subchirps does not result in a lower CRLB as long as the total bandwidth remains the same. Doubling the number of subchirps P, when the bandwidth i.e. B stays the same, leads to a 6.02 dB decrease of the $\mathrm{SINR}_{\mathrm{II}}$ and a four times larger bound.

Similar to the previous section, an alternative representation of the time-delay error bound is found by using the SNR instead of $\mathrm{SINR}_{\mathrm{II}}$, but considering the information loss using the reduced RMS bandwidth. The alternative representation of the time-delay error bound is given by Equation (A.7d) as

$$[\boldsymbol{\mathcal{I}}^{-1}(\boldsymbol{\theta})]_{11} = \left(8\pi^2 \,\mathrm{SNR}\, \tilde{\beta}^2\right)^{-1}\,. \tag{5.55}$$

As seen in Equation (A.12f), the reduced RMS bandwidth $\tilde{\beta}$ for a chirp train-signal with arbitrary starting frequencies is the same as the RMS bandwidth β for the case of a chirp-train signal where each subchirp is symmetric in the frequency domain. Using Equation (A.2c) it can be observed that for the frequency-symmetric chirp case the information-loss term vanishes, which means that the RMS bandwidth reduction is zero.

5.4 DM Case where only the First Phase is Unknown

In the case of a DM process with a single unknown phase caused by the LOS component the signal model from Equation (3.32b) is used with the unknown parameter vector

$$\boldsymbol{\theta} = [\tau, |\alpha|, \arg(\alpha)]^T \ . \tag{5.56}$$

Using the results from [6] the time-delay error bound is written as

$$[\boldsymbol{\mathcal{I}}^{-1}(\boldsymbol{\theta})]_{11} = \left(2\frac{|\alpha|^2}{\sigma_w^2} \left(\|\dot{\boldsymbol{s}}\|_{\mathcal{H}}^2 - \frac{|\langle \dot{\boldsymbol{s}}, \boldsymbol{s} \rangle_{\mathcal{H}}|^2}{\|\boldsymbol{s}\|_{\mathcal{H}}^2} \right) + \mathrm{tr}[\bullet] \right)^{-1} , \tag{5.57}$$

where

$$\mathrm{tr}[\bullet] = \mathrm{tr}\left[\boldsymbol{C}_n^{-1} \frac{\partial \boldsymbol{C}_n}{\partial \tau} \boldsymbol{C}_n^{-1} \frac{\partial \boldsymbol{C}_n}{\partial \tau} \right] , \tag{5.58}$$

and

$$\langle a, b \rangle_{\mathcal{H}} = \sigma_w^2 \boldsymbol{b}^H \boldsymbol{C}_{n,-\tau}^{-1} \boldsymbol{a} \ , \tag{5.59}$$

is the defined inner product in the Hilbert space $\mathcal{H}$ according to [6]. Furthermore,

$$\begin{aligned} \boldsymbol{C}_{n,-\tau}^{-1} &= \mathbb{E}\left[\left(\boldsymbol{W}^H \boldsymbol{P}(-\tau) \boldsymbol{W} \boldsymbol{n} \right) \left(\boldsymbol{W}^H \boldsymbol{P}(-\tau) \boldsymbol{W} \boldsymbol{n} \right)^H \right]^{-1} && \text{(5.60a)} \\ &= \boldsymbol{W}^H \boldsymbol{P}(-\tau) \boldsymbol{W} \boldsymbol{C}_n^{-1} \boldsymbol{W}^H \boldsymbol{P}^H(-\tau) \boldsymbol{W} && \text{(5.60b)} \\ &= \boldsymbol{W}^H \boldsymbol{P}^H(\tau) \boldsymbol{W} \boldsymbol{C}_n^{-1} \boldsymbol{W}^H \boldsymbol{P}(\tau) \boldsymbol{W} \ . && \text{(5.60c)} \end{aligned}$$

is the covariance matrix of the $-\tau$ shifted noise vector $\boldsymbol{n}$. Since the PDP was already shifted by τ it means that $\boldsymbol{C}_{n,-\tau}^{-1}$ is the covariance matrix of the zero-shifted DM process including AWGN. An alternative representation of Equation (5.57) can be found by multiplying the first term with the

mean-square bandwidth β^2 from Equation (5.6) which evaluates to

$$[\boldsymbol{\mathcal{I}}^{-1}(\boldsymbol{\theta})]_{11} = \left(2\frac{\beta^2}{\beta^2}\frac{|\alpha|^2}{\sigma_w^2}\left(\|\dot{\boldsymbol{s}}\|_{\mathcal{H}}^2 - \frac{|\langle\dot{\boldsymbol{s}},\boldsymbol{s}\rangle_{\mathcal{H}}|^2}{\|\boldsymbol{s}\|_{\mathcal{H}}^2}\right) + \mathrm{tr}[\bullet]\right)^{-1} \tag{5.61}$$

$$= \left(8\pi^2\beta^2\frac{|\alpha|^2\|\boldsymbol{s}\|^2}{\sigma_w^2}\left(\frac{\|\dot{\boldsymbol{s}}\|_{\mathcal{H}}^2}{\|\dot{\boldsymbol{s}}\|^2} - \frac{|\langle\dot{\boldsymbol{s}},\boldsymbol{s}\rangle_{\mathcal{H}}|^2}{\|\dot{\boldsymbol{s}}\|^2\|\boldsymbol{s}\|_{\mathcal{H}}^2}\right) + \mathrm{tr}[\bullet]\right)^{-1} \tag{5.62}$$

$$= \left(8\pi^2\beta^2\mathrm{SINR}_{\mathrm{III}} + \mathrm{tr}[\bullet]\right)^{-1}, \tag{5.63}$$

where

$$\mathrm{SINR}_{\mathrm{III}} = \frac{|\alpha|^2\|\boldsymbol{s}\|^2}{\sigma_w^2}\left(\frac{\|\dot{\boldsymbol{s}}\|_{\mathcal{H}}^2}{\|\dot{\boldsymbol{s}}\|^2} - \frac{|\langle\dot{\boldsymbol{s}},\boldsymbol{s}\rangle_{\mathcal{H}}|^2}{\|\dot{\boldsymbol{s}}\|^2\|\boldsymbol{s}\|_{\mathcal{H}}^2}\right), \tag{5.64}$$

is the AWGN equivalent SINR. It is assumed that the additional time delay information $\mathrm{tr}[\bullet]$, which is mainly caused by the increased received signal length due to the convolution of the chirp-train signal with the DM, is negligibly small for high SNR values in comparison to the first term in Equation (5.63) [6].

5.5 DM Case Where all Phases are Unknown

Finally, a DM process where all phases of the train signal are unknown is considered according to Equation (3.35). The unknown parameter vector is

$$\boldsymbol{\theta} = [\tau, |\alpha|, \boldsymbol{\phi}]^T \ , \tag{5.65}$$

and the mean is the same as in Equation (5.30). Using Equation (2.5) the FIM can be calculated. As the noise vector $\boldsymbol{n}$ already has unknown phases due to the DM and the AWGN, it is assumed that the covariance matrix $\boldsymbol{C}_n$ does not depend on the phases $\boldsymbol{\phi}$. The FIM element for the time delay τ is:

$$\begin{aligned}
[\boldsymbol{\mathcal{I}}(\boldsymbol{\theta})]_{11} &= 2\,\mathrm{Re}\left\{ \left(\frac{\partial \boldsymbol{\mu}(\boldsymbol{\theta})}{\partial \tau} \right)^H \boldsymbol{C}_n^{-1} \frac{\partial \boldsymbol{\mu}(\boldsymbol{\theta})}{\partial \tau} \right\} + \mathrm{tr}[\bullet] && \text{(5.66a)} \\
&= 2\,\mathrm{Re}\left\{ |\alpha|^2 \boldsymbol{s}^H \boldsymbol{W}^H \boldsymbol{D}^H \boldsymbol{W} \boldsymbol{C}_{n,-\tau}^{-1} \boldsymbol{W}^H \boldsymbol{D} \boldsymbol{W} \boldsymbol{s} \right\} + \mathrm{tr}[\bullet] && \text{(5.66b)} \\
&= 2\,\mathrm{Re}\left\{ |\alpha|^2 \boldsymbol{s}^H \boldsymbol{C}_{n,-\tau}^{-1} \boldsymbol{s} \right\} + \mathrm{tr}[\bullet] && \text{(5.66c)} \\
&= 2|\alpha|^2 \dot{\boldsymbol{s}}^H \boldsymbol{C}_{n,-\tau}^{-1} \dot{\boldsymbol{s}} + \mathrm{tr}[\bullet] && \text{(5.66d)} \\
&= \frac{2|\alpha|^2}{\sigma_w^2} \|\dot{\boldsymbol{s}}\|_{\mathcal{H}}^2 + \mathrm{tr}[\bullet] \ . && \text{(5.66e)}
\end{aligned}$$

Equation (5.66d) is rewritten to Equation (5.66e) due to the definition of the inner product in the Hilbert space from Equation (5.59). Equation (5.66b) exploits the time shifting property of the covariance matrix from Equation (5.60c) and the time derivative property from Equation (5.14). From Equation (5.66e) it can be seen that the information for the time delay is provided by the signal energy of the time derivative chirp-train signal in the Hilbert space $\mathcal{H}$. For the magnitude $|\alpha|$ of the LOS channel coefficient the FIM element evaluates to

$$\begin{aligned}
[\boldsymbol{\mathcal{I}}(\boldsymbol{\theta})]_{22} &= 2\,\mathrm{Re}\left\{ \left(\frac{\partial \boldsymbol{\mu}(\boldsymbol{\theta})}{\partial |\alpha|} \right)^H \boldsymbol{C}_n^{-1} \frac{\partial \boldsymbol{\mu}(\boldsymbol{\theta})}{\partial |\alpha|} \right\} && \text{(5.67a)} \\
&= 2\boldsymbol{s}^H \boldsymbol{C}_{n,-\tau}^{-1} \boldsymbol{s} && \text{(5.67b)} \\
&= \frac{2}{\sigma_w^2} \|\boldsymbol{s}\|_{\mathcal{H}}^2 \ . && \text{(5.67c)}
\end{aligned}$$

The signal energy in the Hilbert space $\mathcal{H}$ is responsible for the information of the magnitude. For the phases ϕ of the train signal model the corresponding FIM entry is calculated as

$$[\mathcal{I}(\boldsymbol{\theta})]_{33} = 2\,\mathrm{Re}\left\{ \left(\frac{\partial \boldsymbol{\mu}(\boldsymbol{\theta})}{\partial \phi} \right)^H \boldsymbol{C}_n^{-1} \frac{\partial \boldsymbol{\mu}(\boldsymbol{\theta})}{\partial \phi} \right\} \tag{5.68a}$$

$$= 2|\alpha|^2\,\mathrm{Re}\left\{ \mathrm{diag}(\boldsymbol{p})^H \boldsymbol{X}^H \boldsymbol{C}_{n,-\tau}^{-1} \boldsymbol{X}\,\mathrm{diag}(\boldsymbol{p}) \right\} \tag{5.68b}$$

$$= 2|\alpha|^2\,\mathrm{Re}\left\{ \boldsymbol{S}^H \boldsymbol{C}_{n,-\tau}^{-1} \boldsymbol{S} \right\} \tag{5.68c}$$

$$= \frac{2|\alpha|^2}{\sigma_w^2}\,\mathrm{Re}\{\langle \boldsymbol{S}, \boldsymbol{S} \rangle_{\mathcal{H}}\}\,. \tag{5.68d}$$

Equation (5.68b) simplifies to Equation (5.68c) using the matrix $\boldsymbol{S}$ from Equation (3.13). The information of the i-th phase is provided by the signal energy of the i-th subchirp in the Hilbert space $\mathcal{H}$. For the time delay τ and the magnitude $|\alpha|$ of the LOS channel coefficient the corresponding FIM element evaluates to

$$[\mathcal{I}(\boldsymbol{\theta})]_{12} = 2\,\mathrm{Re}\left\{ \left(\frac{\partial \boldsymbol{\mu}(\boldsymbol{\theta})}{\partial \tau} \right)^H \boldsymbol{C}_n^{-1} \frac{\partial \boldsymbol{\mu}(\boldsymbol{\theta})}{\partial |\alpha|} \right\} \tag{5.69a}$$

$$= -2|\alpha|\,\mathrm{Re}\left\{ \boldsymbol{s}^H \boldsymbol{W}^H \boldsymbol{D}^H \boldsymbol{W} \boldsymbol{C}_{n,-\tau}^{-1} \boldsymbol{s} \right\} \tag{5.69b}$$

$$= -2|\alpha|\,\mathrm{Re}\left\{ \dot{\boldsymbol{s}}^H \boldsymbol{C}_{n,-\tau}^{-1} \boldsymbol{s} \right\} \tag{5.69c}$$

$$= -\frac{2|\alpha|}{\sigma_w^2}\,\mathrm{Re}\{\langle \boldsymbol{s}, \dot{\boldsymbol{s}} \rangle_{\mathcal{H}}\}\,. \tag{5.69d}$$

In Equation (5.69b) the time derivative property from Equation (5.14) is again exploited. For the time delay τ and the phases ϕ of the train signal model the FIM entry calculates to

$$[\mathcal{I}(\boldsymbol{\theta})]_{13} = 2\,\mathrm{Re}\left\{ \left(\frac{\partial \boldsymbol{\mu}(\boldsymbol{\theta})}{\partial \tau} \right)^H \boldsymbol{C}_n^{-1} \frac{\partial \boldsymbol{\mu}(\boldsymbol{\theta})}{\partial \phi} \right\} \tag{5.70a}$$

$$= 2|\alpha|^2\,\mathrm{Im}\left\{ \dot{\boldsymbol{s}}^H \boldsymbol{C}_{n,-\tau}^{-1} \boldsymbol{S} \right\} \tag{5.70b}$$

$$= \frac{2|\alpha|^2}{\sigma_w^2}\,\mathrm{Im}\{\langle \boldsymbol{S}, \dot{\boldsymbol{s}} \rangle_{\mathcal{H}}\}\,. \tag{5.70c}$$

For the magnitude $|\alpha|$ of the LOS channel coefficient and the phases ϕ of the train signal model the FIM element is written as

$$[\mathcal{I}(\boldsymbol{\theta})]_{23} = 2\,\mathrm{Re}\left\{\left(\frac{\partial \boldsymbol{\mu}(\boldsymbol{\theta})}{\partial |\alpha|}\right)^H \frac{\partial \boldsymbol{\mu}(\boldsymbol{\theta})}{\partial \boldsymbol{\phi}}\right\} \tag{5.71a}$$

$$= -2|\alpha|\,\mathrm{Im}\left\{\boldsymbol{s}^H \boldsymbol{C}_{n,-\tau}^{-1} \boldsymbol{S}\right\} \tag{5.71b}$$

$$= -\frac{2|\alpha|}{\sigma_w^2}\,\mathrm{Im}\{\langle \boldsymbol{S}, \boldsymbol{s}\rangle_{\mathcal{H}}\}\,. \tag{5.71c}$$

The time-delay error bound is again calculated using the Schur complement similar to Equation (5.21) as

$$[\mathcal{I}^{-1}(\boldsymbol{\theta})]_{11} = \left(2\frac{|\alpha|^2}{\sigma_w^2}\left(F - \boldsymbol{G}\boldsymbol{H}^{-1}\boldsymbol{G}^T\right)\right)^{-1} \tag{5.72}$$

with

$$F = |\alpha|^2 \|\dot{\boldsymbol{s}}\|_{\mathcal{H}}^2 + \frac{\sigma_w^2}{2|\alpha|^2}\,\mathrm{tr}[\bullet] \in \mathbb{R}\,, \tag{5.73}$$

$$\boldsymbol{G} = [-\mathrm{Re}\{\langle \boldsymbol{s}, \dot{\boldsymbol{s}}\rangle_{\mathcal{H}}\}, |\alpha|\,\mathrm{Im}\{\langle \boldsymbol{S}, \dot{\boldsymbol{s}}\rangle_{\mathcal{H}}\}] \in \mathbb{R}^{1\times(P+1))}\,, \tag{5.74}$$

and

$$\boldsymbol{H} = \begin{bmatrix} \|\boldsymbol{s}\|_{\mathcal{H}}^2 & -|\alpha|\,\mathrm{Im}\{\langle \boldsymbol{S}, \boldsymbol{s}\rangle_{\mathcal{H}}\} \\ -|\alpha|\,\mathrm{Im}\{\langle \boldsymbol{S}, \boldsymbol{s}\rangle_{\mathcal{H}}\}^T & |\alpha|^2\,\mathrm{Re}\{\langle \boldsymbol{S}, \boldsymbol{S}\rangle_{\mathcal{H}}\} \end{bmatrix} \in \mathbb{R}^{(P+1)\times(P+1)}\,. \tag{5.75}$$

Therefore, Equation (5.72) is rewritten as

$$[\mathcal{I}^{-1}(\boldsymbol{\theta})]_{11} = \left(2\frac{|\alpha|^2}{\sigma_w^2}\left(\|\dot{\boldsymbol{s}}\|_{\mathcal{H}}^2 - \boldsymbol{G}\boldsymbol{H}^{-1}\boldsymbol{G}^T\right) + \mathrm{tr}[\bullet]\right)^{-1}\,. \tag{5.76}$$

It can be seen that the time-delay error bound from Equation (5.76) has a similar structure as Equation (5.57) except the different subtractive term which accounts for the unknown phases ϕ of the chirp-train signal. It should be noted that the time-delay error bound in general depends on those phase shifts.

Similar to Equation (5.63) an alternative representation can be found by multiplying and dividing the first term with the mean-square bandwidth β^2 from Equation (5.6) which evaluates to

$$[\boldsymbol{\mathcal{I}}^{-1}(\boldsymbol{\theta})]_{11} = \left(2\frac{\beta^2}{\beta^2}\frac{|\alpha|^2}{\sigma_w^2}\left(\|\dot{\boldsymbol{s}}\|_{\mathcal{H}}^2 - \boldsymbol{G}\boldsymbol{H}^{-1}\boldsymbol{G}\right) + \mathrm{tr}[\bullet]\right)^{-1} \tag{5.77}$$

$$= \left(8\pi^2\beta^2\frac{|\alpha|^2\|\boldsymbol{s}\|^2}{\sigma_w^2}\left(\frac{\|\dot{\boldsymbol{s}}\|_{\mathcal{H}}^2}{\|\dot{\boldsymbol{s}}\|^2} - \frac{1}{\|\dot{\boldsymbol{s}}\|^2}\boldsymbol{G}\boldsymbol{H}^{-1}\boldsymbol{G}^T\right) + \mathrm{tr}[\bullet]\right)^{-1} \tag{5.78}$$

$$= \left(8\pi^2\beta^2\mathrm{SINR}_{\mathrm{IV}} + \mathrm{tr}[\bullet]\right)^{-1}, \tag{5.79}$$

where

$$\mathrm{SINR}_{\mathrm{IV}} = \frac{|\alpha|^2\|\boldsymbol{s}\|^2}{\sigma_w^2}\left(\frac{\|\dot{\boldsymbol{s}}\|_{\mathcal{H}}^2}{\|\dot{\boldsymbol{s}}\|^2} - \frac{1}{\|\dot{\boldsymbol{s}}\|^2}\boldsymbol{G}\boldsymbol{H}^{-1}\boldsymbol{G}^T\right), \tag{5.80}$$

is the AWGN equivalent SINR for the DM case where all phases of the chirp-train signal are unknown.

6 Time Delay Estimation and Algorithms

6.1 Maximum Likelihood Time Delay Estimation for the AWGN Case

The maximum likelihood estimator is used for the signal model from Equation (3.28) to find the unknown parameters for the AWGN case. The cost function is defined as

$$J(\tilde{\tau}, |\tilde{\alpha}|, \tilde{\boldsymbol{p}}) = \|\boldsymbol{r} - |\tilde{\alpha}|\boldsymbol{W}^H\boldsymbol{P}(\tilde{\tau})\boldsymbol{W}\boldsymbol{X}\tilde{\boldsymbol{p}}\|^2 \tag{6.1a}$$

$$= \|\boldsymbol{r}\|^2 + |\tilde{\alpha}|^2\|\tilde{\boldsymbol{s}}_{\tilde{\tau},\tilde{\boldsymbol{p}}}\|^2 - 2|\tilde{\alpha}|\,\mathrm{Re}\left\{\tilde{\boldsymbol{s}}^H_{\tilde{\tau},\tilde{\boldsymbol{p}}}\boldsymbol{r}\right\} \tag{6.1b}$$

$$= \|\boldsymbol{r}\|^2 + |\tilde{\alpha}|^2\|\boldsymbol{x}\|^2 - 2|\tilde{\alpha}|\,\mathrm{Re}\left\{\tilde{\boldsymbol{s}}^H_{\tilde{\tau},\tilde{\boldsymbol{p}}}\boldsymbol{r}\right\}, \tag{6.1c}$$

where

$$\tilde{\boldsymbol{s}}_{\tilde{\tau},\tilde{\boldsymbol{p}}} = \boldsymbol{W}^H\boldsymbol{P}(\tilde{\tau})\boldsymbol{W}\boldsymbol{X}\tilde{\boldsymbol{p}}\,, \tag{6.2}$$

is the by $\tilde{\tau}$ delayed and phase shifted template chirp train signal. For some $\tilde{\tau}$ the cost function can be minimized by inserting $\boldsymbol{W}^H\boldsymbol{P}(\tilde{\tau})\boldsymbol{W}\boldsymbol{X}$ into Equation (2.12) which leads to

$$|\hat{\alpha}|\hat{\boldsymbol{p}} = (\boldsymbol{X}^H\boldsymbol{X})^{-1}(\boldsymbol{W}^H\boldsymbol{P}(\tilde{\tau})\boldsymbol{W}\boldsymbol{X})^H\boldsymbol{r} \tag{6.3}$$

$$= \frac{1}{N_c}(\boldsymbol{W}^H\boldsymbol{P}(\tilde{\tau})\boldsymbol{W}\boldsymbol{X})^H\boldsymbol{r}\,. \tag{6.4}$$

The phases $\hat{\phi}$ of the chirp train signal are calculated as

$$\hat{\phi} = \arg\left(\left(\boldsymbol{W}^H\boldsymbol{P}(\tilde{\tau})\boldsymbol{W}\boldsymbol{X}\right)^H\boldsymbol{r}\right)\,. \tag{6.5}$$

Therefore, the individual phases ϕ_i can be calculated as

$$\hat{\phi}_i = \arg\left(\sum_{n=0}^{N_c-1} x_i^*(nT_s - \tilde{\tau})r[iN_c + n]\right) . \tag{6.6}$$

The ML magnitude estimate $|\hat{\alpha}|$ of the LOS channel coefficient can be obtained by multiplying the phase vector estimate $\hat{\boldsymbol{p}}^H$ with Equation (6.4). This leads to the amplitude estimate

$$|\hat{\alpha}| = \frac{1}{N}\hat{\boldsymbol{s}}_{\tilde{\tau},\hat{\boldsymbol{p}}}\,\boldsymbol{r} . \tag{6.7}$$

The ML estimate for the time delay τ can be found by minimizing the cost function from Equation (6.1b) as

$$\hat{\tau} = \arg\min_{\tilde{\tau},|\tilde{\alpha}|,\tilde{\phi}} \{J(\tilde{\tau}, |\tilde{\alpha}|, \tilde{\boldsymbol{p}})\} \tag{6.8}$$

$$= \arg\min_{\tilde{\tau},|\tilde{\alpha}|,\tilde{\phi}} \left\{\|\boldsymbol{r} - |\tilde{\alpha}|\tilde{\boldsymbol{s}}_{\tilde{\tau},\tilde{\boldsymbol{p}}}\|^2\right\} \tag{6.9}$$

$$= \arg\min_{\tilde{\tau}} \left\{\min_{|\tilde{\alpha}|,\tilde{\phi}} \left\{\|\boldsymbol{r} - |\tilde{\alpha}|\tilde{\boldsymbol{s}}_{\tilde{\tau},\tilde{\boldsymbol{p}}}\|^2\right\}\right\} . \tag{6.10}$$

It should be noted that the joint minimization can be split into an inner and an outer minimization. The inner minimization is achieved by calculating the phase estimates $\hat{\phi}$ and the amplitude estimate $|\hat{\alpha}|$ according to Equations (6.5) and (6.7) for each $\tilde{\tau}$.

A second Maximum Likelihood estimator can be found when considering a downconverted signal. First of all a unitary transformation matrix for the downconversion is defined as

$$\boldsymbol{U}^H = \mathrm{diag}\left(\left[-j2\pi\left(\frac{mn^2}{2} + f_0 n\right)\right]_{n=0}^{M-1}\right) . \tag{6.11}$$

In contrast to Section (4.4) only one large chirp is used for the downconversion instead of the template chirp train. Equation (6.10) can be modified as

$$\hat{\tau} = \arg\min_{\tilde{\tau}} \left\{ \min_{|\tilde{\alpha}|,\tilde{\phi}} \left\{ \|\boldsymbol{r} - |\tilde{\alpha}|\tilde{\boldsymbol{s}}_{\tilde{\tau},\tilde{\boldsymbol{p}}}\|^2 \right\} \right\} \tag{6.12a}$$

$$= \arg\min_{\tilde{\tau}} \left\{ \min_{|\tilde{\alpha}|,\tilde{\phi}} \left\{ \|\boldsymbol{U}^H (\boldsymbol{r} - |\tilde{\alpha}|\tilde{\boldsymbol{s}}_{\tilde{\tau},\tilde{\boldsymbol{p}}})\|^2 \right\} \right\} \tag{6.12b}$$

$$= \arg\min_{\tilde{\tau}} \left\{ \min_{|\tilde{\alpha}|,\tilde{\phi}} \left\{ \|\boldsymbol{r}_d - |\tilde{\alpha}|\tilde{\boldsymbol{s}}_{d,\tilde{\tau},\tilde{\boldsymbol{p}}}\|^2 \right\} \right\} , \tag{6.12c}$$

where

$$\boldsymbol{r}_d = \boldsymbol{U}^H \boldsymbol{r} , \tag{6.13}$$

is the downconverted received signal and

$$\tilde{\boldsymbol{s}}_{d,\tilde{\tau},\tilde{\boldsymbol{p}}} = \boldsymbol{U}^H \tilde{\boldsymbol{s}}_{\tilde{\tau},\tilde{\boldsymbol{p}}} , \tag{6.14}$$

is the downconverted, time delayed and phase shifted template chirp train signal. It can be seen that the estimation of the time delay is the same as the estimation of the frequencies of the downconverted signal.

6.2 Time Delay Estimation for the DM Case

As it can be seen from Figure 3.2 the largest peak of the individual multipath components (including the LOS component) does not necessarily correspond to the LOS component which leads to a decreased performance of the AWGN ML estimator. By rewriting Equation (3.31) the received signal in the DM case can be expressed as a sum of multiple time delayed and scaled components where

$$r[n] = \alpha s(nT_s - \tau) + T_s(s * v)[n] + w[n] \tag{6.15}$$

$$= \alpha s(nT_s - \tau) + T_s \sum_{k=0}^{L-1} s[n-k]v[k] + w[n] . \tag{6.16}$$

Similar to [18] an algorithm which tries to find the first component by iteratively estimating and subtracting the individual components, which are shown in Equation (6.16), is presented in the following listing.

Algorithm 1 Search and subtract

Input received signal $\boldsymbol{r}$, chirp train matrix $\boldsymbol{X}$, power threshold, max components
Output min(delays)
procedure
delays $\leftarrow$ [] ▷ Initializes a list for the delays
components $\leftarrow 0$ ▷ In the beginning there are zero components
r$' \leftarrow r$ ▷ Copies the received signal
repeat
$\hat{\tau} \leftarrow \arg\min_{\tilde{\tau}} \left\{ \min_{|\tilde{\alpha}|,\tilde{\phi}} \left\{ \|\boldsymbol{r}' - |\tilde{\alpha}| \tilde{\boldsymbol{s}}_{\tilde{\tau},\tilde{\boldsymbol{p}}} \|^2 \right\} \right\}$ ▷ Calculates ML estimate
$\boldsymbol{r}' \leftarrow \boldsymbol{r}' - \hat{\boldsymbol{s}}^H_{\hat{\tau},\hat{\boldsymbol{p}}} \boldsymbol{r} \hat{\boldsymbol{s}}_{\hat{\tau},\hat{\boldsymbol{p}}}$ ▷ Subtracts the projected component
signal power $\leftarrow \|\boldsymbol{r}'\|^2 / M$ ▷ Calculates the signal power from the subtracted signal
delays[components] $\leftarrow \hat{\tau}$ ▷ Adds the current time delay estimate to the list
components $\leftarrow$ components $+ 1$
until signal power < power threshold **or** components > max components
end procedure

In Listing 1 it can be seen that the algorithm stops if the power level of the subtracted signal $\boldsymbol{r}'$ is below a specific threshold. This is due to the noise floor caused by the AWGN. Furthermore, an error is introduced since the individual projected components are estimated separately. The number of spectral components is therefore used as an additional stopping condition. It should be noted that the same algorithm can be used for the downconverted signal and the time delay estimate from Equation (6.12c). This might result in a better estimate since the downconversion of the multipath components leaves complex sinusoidal signals similar to [19] with different frequencies which are better separable.

7 Simulations

In this chapter, the mean squared error (MSE) values of the different time delay estimation methods from Chapter 6 are investigated using simulations. The simulations are also performed for the CRLBs from Chapter 5 and compared against the performance of the time delay estimation methods. Furthermore, the influence of dividing one long chirp into several subchirps with unknown start phases is analyzed. The signals cover the maximum bandwidth of the CC2510 transceiver chips from Chapter 4 which is 80 MHz. The time delay estimates were found using a grid search with refining for the respective cost functions.

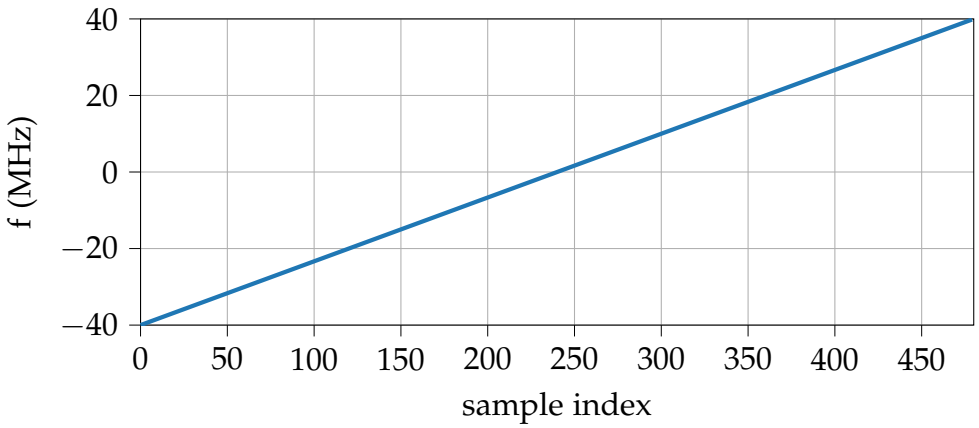

Figure 7.1: Spectrogram of a single chirp with a length of $N = 480$ samples, a sample rate of $f_s = 80$ MHz and a chirp rate of $m = f_s / N$.

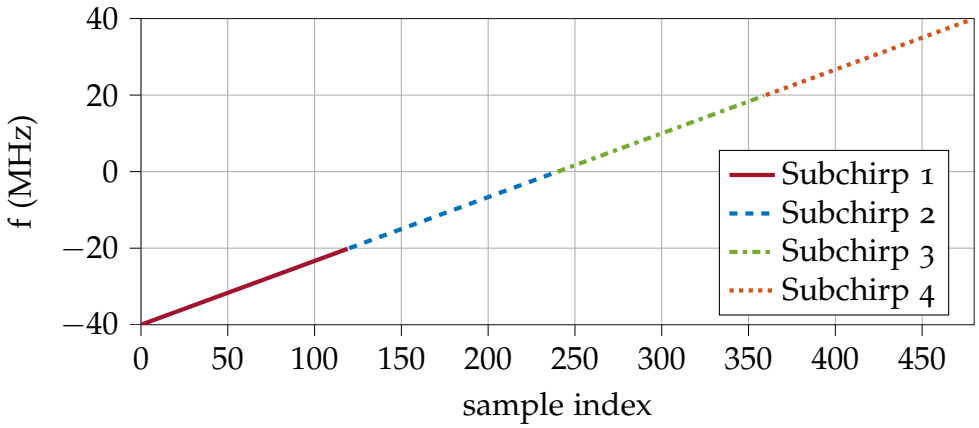

Figure 7.2: Spectrogram of a chirp train with $P = 4$ subchirps, a total length of $N = 480$ samples, a sample rate of $f_s = 80$ MHz, a chirp length of N/P and a chirp rate of $m = f_s/N$.

Figure 7.2 shows the division of a single longer chirp from Figure 7.1 into four smaller chirps of equal length. Since the chirp rate m and the total length N stays the same the bandwidth is also the same as for the single chirp case from Figure 7.1. The following settings and definitions are used in this chapter:

- A sample rate of $f_s = 80$ MHz, an amount of $N = 480$ samples, and a linear chirp rate of $m = f_s/N$ such that the chirp-train signal covers the full bandwidth of 80 MHz.
- An amount of subchirps $P \in \{1, 2, 4, 8\}$ which divides the long single chirp into multiple subchirps with unknown phases.
- The SNR definition from Equation (5.7) is used and the magnitude $|\alpha|$ of the LOS channel coefficient is set to one.

It should be noted that the CRLB in the DM case is calculated using the inverse of a covariance matrix. This matrix is in turn calculated by chirp-train signal oversampled by a factor of 10. Due to the long computing time of the inverse of the covariance matrix, the chirp length is set to $N = 480$ samples. As it can be seen in Appendix A, the number of samples in the AWGN case does not affect the time delay error bound anyway when the bandwidth is fixed.

7.1 AWGN Case

In this section, the time delay error bounds for a different amount of subchirps with unknown start phases from Equation (5.53) are compared to the MSE values of the ML estimates from Section 6.1 for different SNR values. For better comparability, the time delay error bound is converted to the distance error bound by multiplying it with the speed of light.

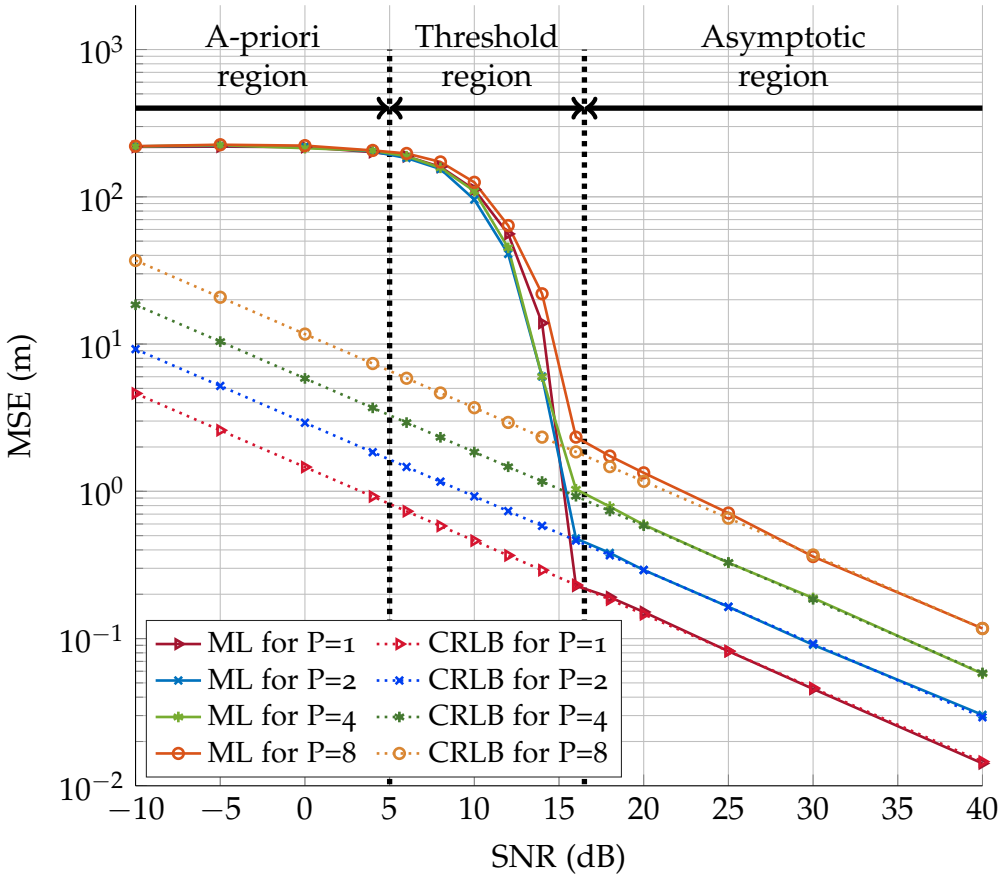

Figure 7.3: Distance error bounds and ML estimation accuracies for a different amount of subchirps P with unknown start phases. A total of 1000 realizations are used and the the search range of the time delay is limited to ± 100 samples. The regions are defined according to [20].

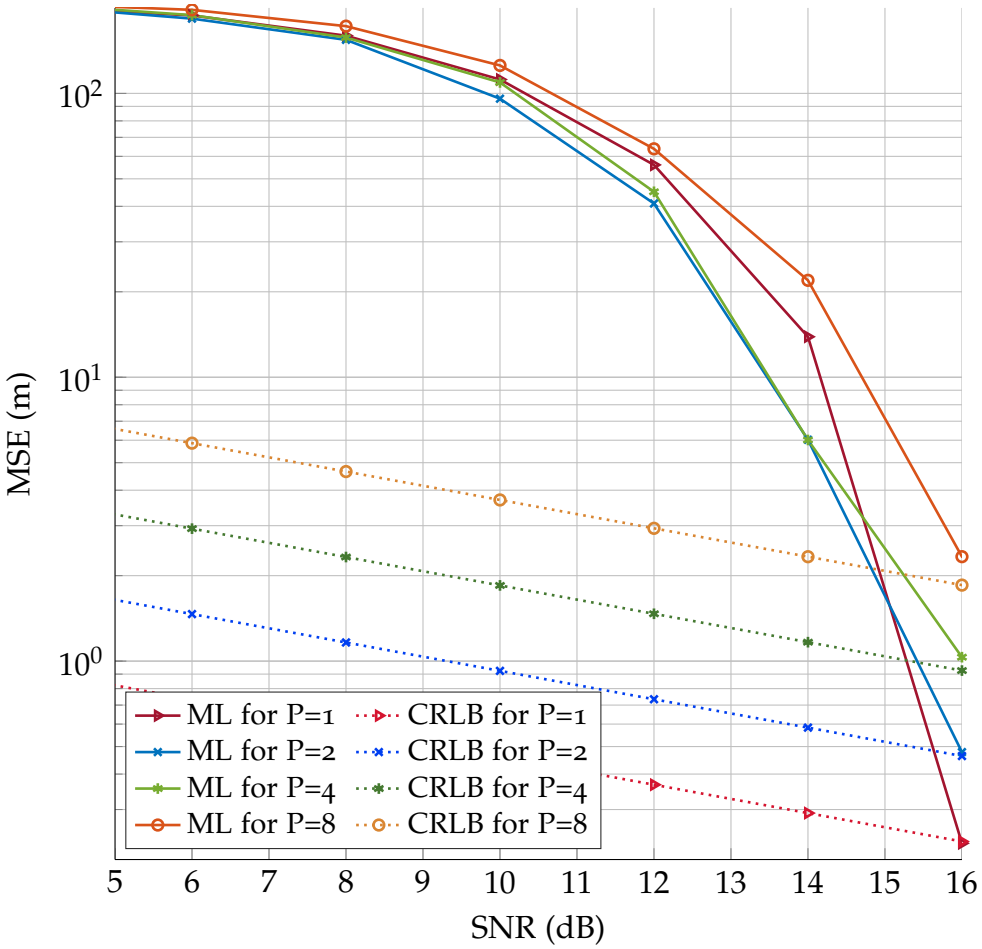

Figure 7.4: Magnification of the threshold region from Figure 7.3.

Figure 7.3 shows that an increase in the amount of subchirps P leads to an increased error bound. It can also be seen that doubling the number of subchirps performs just as well as the non-doubled version with approximately 6 dB less SNR which matches with the 6.02 dB decrease in $\mathrm{SINR}_{\mathrm{II}}$ described in Section 5.3. The different ML estimators converge to their error bounds at an SNR of approximately 16 dB. Similar to [20] the following regions can be observed for any amount of subchirps P:

- A-priori region when SNR $<$ 5 dB: In this region, the signal is not detectable within the noise floor. No information about the time delay can be obtained since the MSE of the estimate is only bounded by the a-priori knowledge of the time delay range and therefore is distributed uniformly. This relates to a signal detection problem. The amount of subchirps P has no influence.
- Threshold region when 5 dB $<$ SNR $<$ 16 dB: Smooth transition between the a-priori region and the asymptotic region. The amount of subchirps P only has a small impact on the MSE. However, the threshold region is shifted further to the right with an increasing amount of subchirps. This happens because the increase in the amount of subchirps can be viewed as a decrease of the $\mathrm{SINR}_{\mathrm{II}}$, which means that a larger SNR is needed for achieving the same $\mathrm{SINR}_{\mathrm{II}}$ for the case of a single chirp. It should be noted that the outlier in the threshold region for a single subchirp, where the MSE is larger than for four subchirps, was probably caused by the discrete grid search and could be avoided by using other optimization algorithms. The magnified version of the threshold region from Figure 7.3 is shown in Figure 7.4.
- Asymptotic region when 16 dB $<$ SNR: The MSE of the MLE reaches the error bound. Doubling the amount of subchirps P leads to a 6.02 dB decrease in $\mathrm{SINR}_{\mathrm{II}}$ and to a four times higher delay error bound as for the non-doubled case.

7.2 DM Case

For the analysis of the DM case the double-exponential PDP from Equation (3.39) is used with the settings $\gamma_r = 5$ ns and $\gamma_d = 20$ ns similar to [11] which corresponds to a typical indoor scenario. The energy normalization factor Ω_1 of the PDP is adjusted so that the Rician K-factor K_{LOS} from Equation (3.44b) has certain values. The time delay error bounds are again converted to the distance error bound. Small K_{LOS} values, for example, -5 dB, correspond to a larger energy of the DM components compared to the LOS energy. Conversely, for large K_{LOS} values, for example, 20 dB, there is more energy in the LOS component than in the DM components.

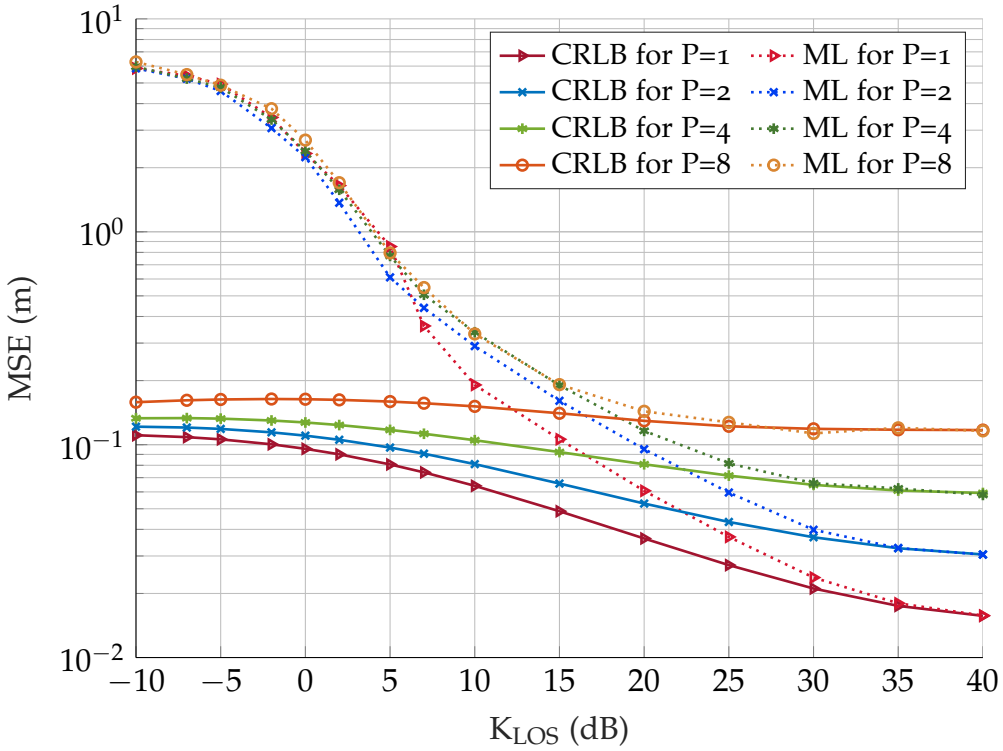

Figure 7.5: Comparison between the distance error bounds and the AWGN estimation accuracies for a different amount of subchirps P with unknown start phases for an SNR of 40 dB. A total of 1000 realizations are used and the the search range of the time delay is limited to ± 40 samples.

Figure 7.5 shows the different error bounds of the distance estimation and the MSE values of the AWGN ML estimator for various Rician K-factors and a different amount of subchirps P. An SNR of 40 dB is used. Similar to Figure 7.3, a threshold region and an asymptotic region can be seen. The asymptotic region is shifted to the right as the amount of subchirps P is increased. The error bounds hardly differ at very low K_{LOS} values. This happens because the DM process already adds unknown phases on the chirp-train signal and unknown start phases do not matter that much anymore. The same behavior can be seen for the AWGN ML estimation accuracies. As the energy of the PDP is increased, the DM process has less influence on the phases of the received chirp-train signal, and the amount of subchirps P becomes more significant. For K_{LOS} values greater than 40 dB, the error bounds of the DM case converge to the error bounds of the AWGN case.

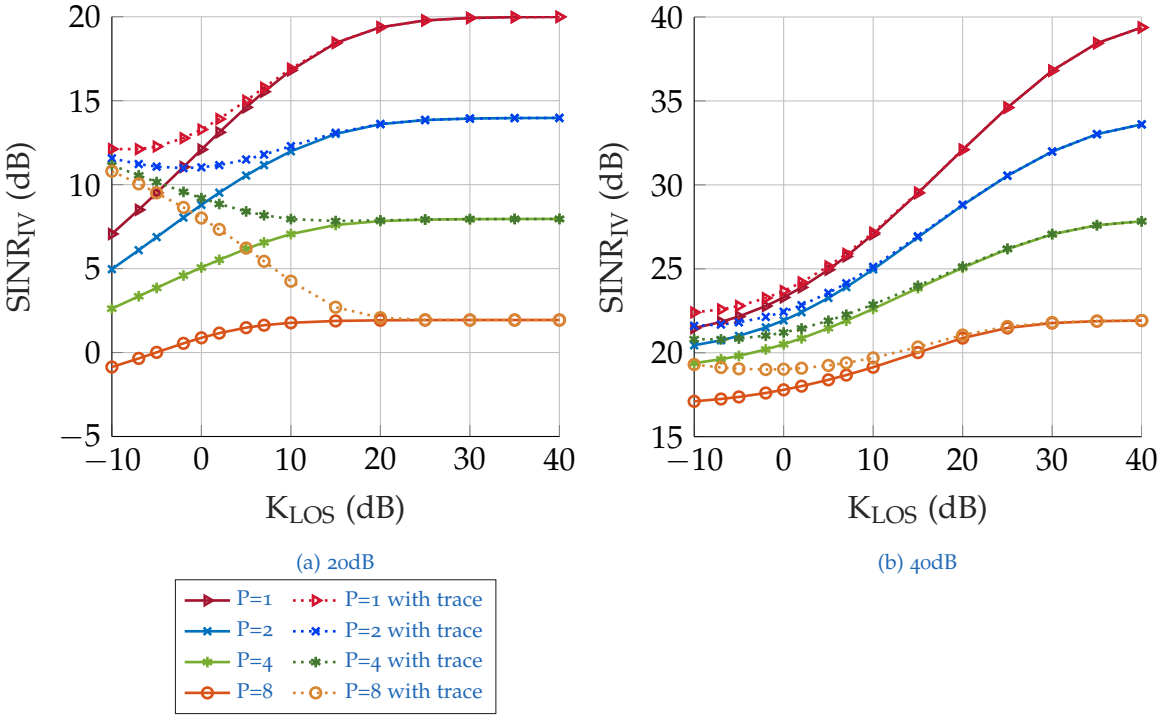

(a) 20dB

(b) 40dB

Figure 7.6: Comparison between $\mathrm{SINR}_{\mathrm{IV}}$ values for a different amount of subchirps P with unknown start phases. A total of 1000 realizations are used. It should be noted that both plots have a different scaling.

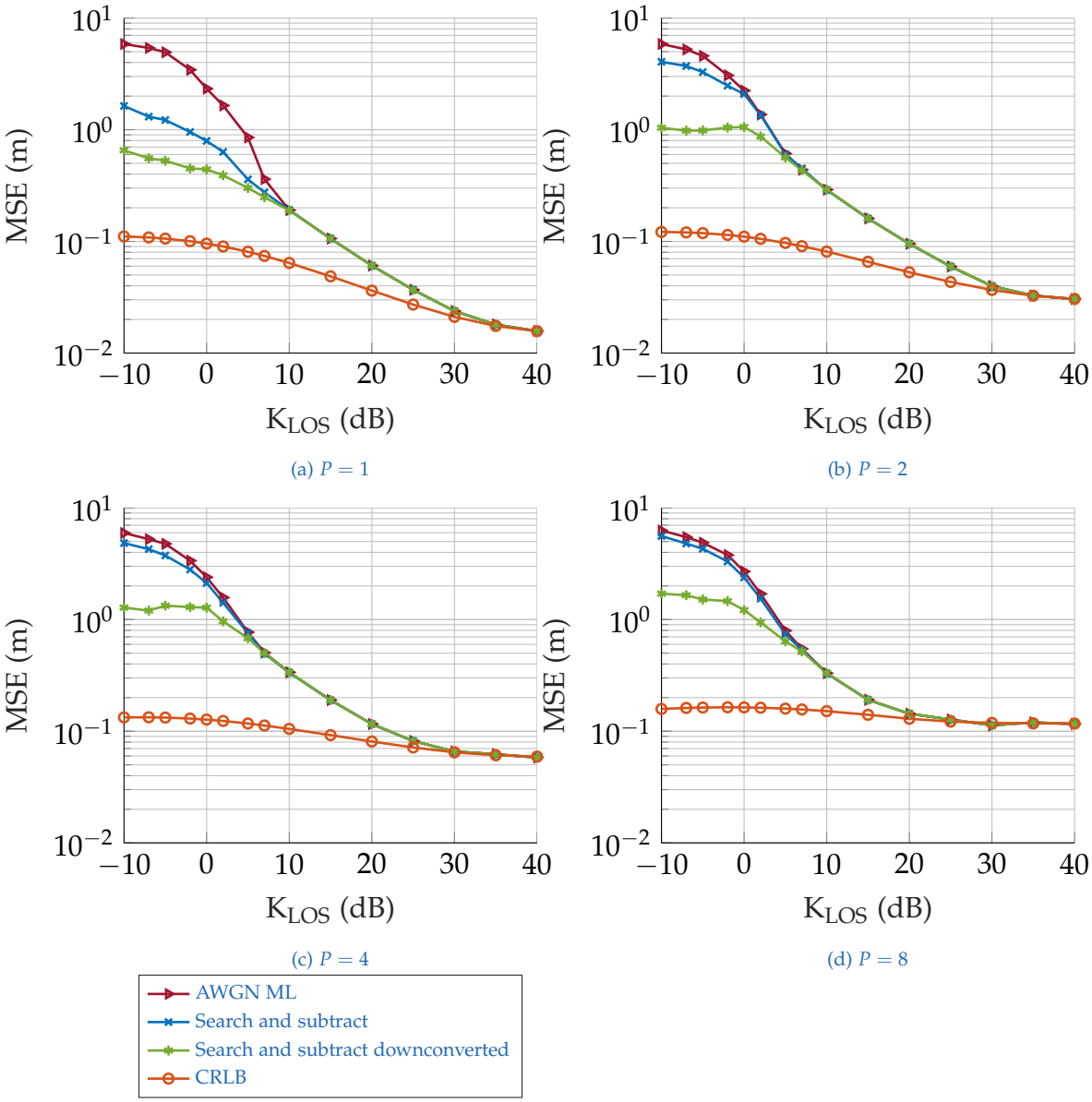

(a) $P = 1$

(b) $P = 2$

(c) $P = 4$

(d) $P = 8$

Figure 7.7: Comparison between the distance error bounds, the AWGN estimation accuracies, and the estimation accuracies of the search and subtract algorithms for a different amount of subchirps P with unknown start phases. An SNR of 40 dB is used together with 1000 realizations. The maximum amount of subtracted components for the search and subtract algorithm is set to 30, the power threshold is set to 0.8 for the normal version, and to 0.3 for the downconverted one.

Figure 7.6 shows the comparison between the SINR_{IV} values for a different amount of subchirps P for SNR values of 20 dB and 40 dB. The SINR_{IV} values have been calculated according to Equation (5.80) for the case which does not consider the trace from Equation (5.58) and for the case where this is taken into account. When there is much energy in the DM components (i.e. K_{LOS} is small) for an SNR of 20 dB, the SINR_{IV} values which consider the trace term are much higher than the ones without it. For the case with the SNR of 40 dB, the information gain caused by the trace term is much smaller. This seems to be the case due to the additional energy caused by the DM components and therefore a better detectability for lower SNR values is given. If much energy is in the DM components (i.e. K_{LOS} is small), for both SNR cases the SINR_{IV} values which consider the trace are almost independent of the amount of subchirps P. In contrast, the number of subchirps P matters more when there is little energy in the DM (i.e. K_{LOS} is large) since it approximates the AWGN case. As the energy of the DM components is increased, the SINR_{IV} values approach the SINR_{II} values for the corresponding amount of subchirps P.

In Figure 7.7 the search and subtract algorithm and the version for the downconverted signal from Section 6.2 are compared to the AWGN ML estimator and the distance error bound. The search and subtract algorithm works hardly better than the AWGN ML estimator with multiple subchirps whereas the search and subtract algorithm for the downconverted signal leads to a significant improvement in accuracy in the threshold region for all subchirp cases. This is because of the better separability of the components. Furthermore, the search and subtract algorithms converge to the AWGN ML estimation MSE at a K_{LOS} of about 10 dB.

In [21] a pulse-compression technique is presented which enables an accurate estimation of the unknown phase differences of the chirp-train signal by using frequency-overlapping subchirps. This is possible due to the frequency-selective filtering done by the DM process, which adds the same unknown phases for the frequency overlaps. This approach also utilizes information from other receivers.

It should be noted that this approach does not result in a significantly better time-delay estimate in the case of a single transmitter and a single receiver. This is evident from Figure 7.5, where the AWGN ML estimator for a single unknown start phase does not perform significantly better than the AWGN ML estimators for multiple unknown start phases when K_{LOS} is low. As K_{LOS} increases, the time delay estimation is more accurate when using the phase estimates instead of phase differences estimates since it will converge to the AWGN case and the AWGN ML estimator is asymptotically efficient.

8 Conclusion

This thesis helps to better understand the problem of introducing multiple unknown start phases for chirp-train signals which are used for time-delay estimation. The theoretical lower bound was derived for time-delay estimation for a chirp-train signal with unknown start phases for the AWGN and the dense multipath (DM) cases. This generalizes the concepts of the single unknown phase cases from the literature. One key finding is that the AWGN equivalent SNR is decreased by 6.02 dB when the number of chirps is doubled, under the assumption that the total bandwidth is fixed and there is no energy in the DM components. It leads to a four-times larger CRLB for the time-delay estimation. As the energy of the DM components increases, the differences in the CRLB for different amounts of subchirps become smaller. This happens because the DM process also causes unknown phases and the effect of the additional unknown start phases of the chirp-train signal is thereby reduced.

It has been shown that the information decrease due to additional estimation parameters can be viewed as a decrease in the effective SINR. Alternatively, the loss of information due to the additional estimation parameters can be viewed as a reduction in root-mean-square (RMS) bandwidth. The reduced RMS bandwidth of a chirp-train signal with arbitrary starting frequencies is the same as the RMS bandwidth for the case of a chirp-train signal where each subchirp is symmetric in the frequency domain. When frequency-symmetric subchirps are considered, the information loss is zero and the reduced RMS bandwidth is equal to the RMS bandwidth.

In simulations, it was shown that the AWGN ML estimator is asymptotically efficient for the AWGN case when the SNR is large enough. Similarly, for the DM case, the AWGN estimator asymptotically reaches the CRLB for comparatively low energies in the DM components. In addition, improvements have been made in the threshold region for the DM case using the search-and subtract-algorithm. Because of the better separability of the components, these improvements were even more significant when using this algorithm on the downconverted signal.

Furthermore, FPGA implementation details were shown for a chirp compression algorithm, which drastically reduces the required bandwidth between the receiver and the host computer. For this purpose, the chirp-train signal was generated on an FPGA using direct digital synthesis (DDS). The complex conjugate of the signal was multiplied with the received chirp-train signal for downconversion, and finally, the result was decimated using filtering and downsampling stages.

Appendix

Appendix A

CRLB simplification for the AWGN case

The CRLB from Equation (5.51b), which considers the AWGN case when all phases of the chirp train signal are unknown, can be simplified. This is done using Equation (3.16b) where the time derivative chirp train vector $\|\dot{\boldsymbol{x}}\|^2$ simplifies to

$$\|\dot{\boldsymbol{x}}\|^2 = 4\pi^2 \sum_{i=0}^{P-1} \sum_{n=0}^{N_c-1} (mn + f_i)^2 \tag{A.1a}$$

$$= 4\pi^2 \sum_{i=0}^{P-1} \sum_{n=0}^{N_c-1} m^2 n^2 + 2mnf_i + f_i^2 \tag{A.1b}$$

$$= 4\pi^2 \sum_{i=0}^{P-1} \frac{m^2}{6} N_c(N_c-1)(2N_c-1) + mN_c(N_c-1)f_i + N_c f_i^2 \tag{A.1c}$$

$$= 4\pi^2 \left(\frac{m^2}{6} PN_c(N_c-1)(2N_c-1) + mN_c(N_c-1) \sum_{i=0}^{P-1} f_i \right.$$
$$\left. + N_c \sum_{i=0}^{P-1} f_i^2 \right) , \tag{A.1d}$$

and the simplification for the subtractive term of the CRLB is

$$\sum_{i=0}^{P-1} \frac{\mathrm{Im}\{\boldsymbol{x}_i^H \dot{\boldsymbol{x}}_i\}^2}{\|\boldsymbol{x}_i\|^2} = \frac{1}{N_c} \sum_{i=0}^{P-1} \mathrm{Im}\left\{\boldsymbol{x}_i^H \dot{\boldsymbol{x}}_i\right\}^2 \tag{A.2a}$$

$$= \frac{4\pi^2}{N_c} \sum_{i=0}^{P-1} \left(\sum_{n=0}^{N_c-1} mn + f_i \right)^2 \tag{A.2b}$$

$$= \frac{4\pi^2}{N_c} \sum_{i=0}^{P-1} \left(\frac{m}{2} N_c(N_c-1) + f_i N_c \right)^2 \tag{A.2c}$$

$$= 4\pi^2 \left(\frac{m^2}{4} P N_c (N_c-1)^2 + m N_c (N_c-1) \sum_{i=0}^{P-1} f_i + N_c \sum_{i=0}^{P-1} f_i^2 \right) . \tag{A.2d}$$

Equations (A.1d) and (A.2d) are inserted into Equation (5.51b) as

$$[\boldsymbol{\mathcal{I}}^{-1}(\boldsymbol{\theta})]_{11} = \frac{\sigma_w^2}{2|\alpha|^2} \left(\|\dot{\boldsymbol{x}}\|^2 - \sum_{i=0}^{P-1} \frac{\mathrm{Im}\{\boldsymbol{x}_i^H \dot{\boldsymbol{x}}_i\}^2}{\|\boldsymbol{x}_i\|^2} \right)^{-1} \tag{A.3a}$$

$$= \frac{\sigma_w^2}{2|\alpha|^2 4\pi^2} \left(\frac{m^2}{6} P N_c (N_c-1)(2N_c-1) - \frac{m^2}{4} P N_c (N_c-1)^2 \right)^{-1} \tag{A.3b}$$

$$= \frac{\sigma_w^2}{2|\alpha|^2 4\pi^2} \left(\frac{1}{12} m^2 P N_c (N_c^2-1) \right)^{-1} \tag{A.3c}$$

$$= \frac{3\sigma_w^2}{2\pi^2 |\alpha|^2 m^2 P N_c (N_c^2-1)} . \tag{A.3d}$$

Using the definition of the SNR with

$$\mathrm{SNR} = \frac{|\alpha|^2 \|\boldsymbol{x}\|^2}{\sigma_w^2} , \tag{A.4}$$

Equation (A.3d) simplifies to

$$[\boldsymbol{\mathcal{I}}^{-1}(\boldsymbol{\theta})]_{11} = \frac{3}{2\pi^2 \,\mathrm{SNR}\, m^2 (N_c^2-1)} . \tag{A.5}$$

Since the length of a subchirp N_c is typically long i.e.

$$N_c^2 - 1 \approx N_c^2 \,, \tag{A.6}$$

Equation (A.5) can be approximated as

$$[\boldsymbol{\mathcal{I}}^{-1}(\boldsymbol{\theta})]_{11} = \frac{3}{2\pi^2 \,\mathrm{SNR}\, m^2 N_c^2} \tag{A.7a}$$

$$= \frac{3P^2}{2\pi^2 \,\mathrm{SNR}\, B^2} \tag{A.7b}$$

$$= \frac{12P^2}{8\pi^2 \,\mathrm{SNR}\, B^2} \tag{A.7c}$$

$$= \left(8\pi^2 \,\mathrm{SNR}\, \tilde{\beta}^2\right)^{-1} \,, \tag{A.7d}$$

where

$$B = mN \,, \tag{A.8}$$

is the absolute bandwidth a single chirp of length N and the linear chirp rate m would achieve,

$$B_c = \frac{B}{P} \,, \tag{A.9}$$

is the bandwidth a subchirp achieves and

$$\tilde{\beta} = \frac{B_c}{\sqrt{12}} \,, \tag{A.10}$$

is the reduced root-mean-square (RMS) bandwidth. Based on simulations, it can be determined that the reduced RMS bandwidth $\tilde{\beta}$ is equal to the RMS bandwidth β for a chirp-train signal where each subchirp is symmetric in the frequency domain i.e. the start frequency of the i-th subchirp is

$$f_i = -\frac{mN_c}{2} \quad 0 \leq i < P \,. \tag{A.11}$$

To verify this statement, the mean-square bandwidth β^2 is calculated for this case by inserting Equation (A.1d) into Equation (5.6) as

$$\beta^2 = \frac{\|\dot{\boldsymbol{x}}\|^2}{4\pi^2\|\boldsymbol{x}\|^2} \tag{A.12a}$$

$$= \frac{1}{N_c P}\left(\frac{m^2 P N_c^3}{3} + mN_c^2\sum_{i=0}^{P-1} f_i + N_c\sum_{i=0}^{P-1} f_i^2\right) \tag{A.12b}$$

$$= \frac{1}{N_c P}\left(\frac{m^2 P N_c^3}{3} - \frac{m^2 P N_c^3}{2} + \frac{m^2 P N_c^3}{4}\right) \tag{A.12c}$$

$$= \frac{m^2 N_c^2}{12} \tag{A.12d}$$

$$= \frac{B^2}{12P} \tag{A.12e}$$

$$= \frac{B_c^2}{12}\,, \tag{A.12f}$$

which is in fact equal to the reduced mean-square bandwidth $\tilde{\beta}^2$. It should be noted that the simplification from Equation (A.6) was also used for this derivation.

Bibliography

[1] Davide Dardari et al. "Ranging With Ultrawide Bandwidth Signals in Multipath Environments." In: *Proceedings of the IEEE* 97.2 (2009), pp. 404–426. DOI: 10.1109/JPROC.2008.2008846 (cit. on pp. 1, 14).

[2] Heein Yang et al. "Implementation of DDS chirp signal generator on FPGA." In: *2014 International Conference on Information and Communication Technology Convergence (ICTC)*. 2014, pp. 956–959. DOI: 10.1109/ICTC.2014.6983343 (cit. on pp. 1, 29).

[3] Daniel Neunteufel et al. "Coherent Chirp Generation by Narrowband Transceiver Chips for ToF Indoor Localization." In: *GLOBECOM 2020 - 2020 IEEE Global Communications Conference*. 2020, pp. 1–6. DOI: 10.1109/GLOBECOM42002.2020.9348025 (cit. on pp. 1, 21, 24).

[4] F. McGroary and K. Lindell. "A stepped chirp technique for range resolution enhancement." In: *NTC '91 - National Telesystems Conference Proceedings*. 1991, pp. 121–126. DOI: 10.1109/NTC.1991.147999 (cit. on p. 1).

[5] S. M. Kay. *Fundamentals of Statistical Signal Processing: Estimation Theory*. Prentice Hall, 1997 (cit. on pp. 2, 5–7, 35, 36).

[6] Klaus Witrisal et al. "Bandwidth Scaling and Diversity Gain for Ranging and Positioning in Dense Multipath Channels." In: *IEEE Wireless Communications Letters* 5.4 (2016), pp. 396–399. DOI: 10.1109/LWC.2016.2569087 (cit. on pp. 2, 14, 36, 47, 48).

[7] José A. del Peral-Rosado et al. "Joint channel and time delay estimation for LTE positioning reference signals." In: *2012 6th ESA Workshop on Satellite Navigation Technologies (Navitec 2012) & European Workshop on GNSS Signals and Signal Processing*. 2012, pp. 1–8. DOI: 10.1109/NAVITEC.2012.6423094 (cit. on pp. 8, 13).

[8] Dehan Luan. *Fundamental Performance Limits on Time of Arrival Estimation Accuracy with 5G Radio Access*. Master's thesis. Available at http://www.diva-portal.org/smash/get/diva2:1182120/FULLTEXT01.pdf. 2017 (cit. on pp. 13, 15).

[9] Samira Boualleg and Brahim Haraoubia. "Influence of multipath radio propagation on wideband channel transmission." In: *International Multi-Conference on Systems, Signals & Devices*. 2012, pp. 1–6. DOI: 10.1109/SSD.2012.6197993 (cit. on p. 14).

[10] Erik Leitinger et al. "Evaluation of Position-Related Information in Multipath Components for Indoor Positioning." In: *IEEE Journal on Selected Areas in Communications* 33.11 (2015), pp. 2313–2328. DOI: 10.1109/JSAC.2015.2430520 (cit. on p. 14).

[11] Andreas Fuchs and Klaus Witrisal. "Time-of-Arrival Estimation for Positioning in Bandwidth-Limited Dense Multipath Channels." In: *2022 IEEE 23rd International Workshop on Signal Processing Advances in Wireless Communication (SPAWC)*. 2022, pp. 1–5. DOI: 10.1109/SPAWC51304.2022.9833995 (cit. on pp. 15–17, 62).

[12] Thomas Wilding et al. "Accuracy Bounds for Array-Based Positioning in Dense Multipath Channels." In: *Sensors* 18 (Dec. 2018), p. 4249. DOI: 10.3390/s18124249 (cit. on pp. 15, 39).

[13] Daniel Neunteufel. "Indoor positioning of low-cost narrowband IoT nodes." PhD thesis. Technische Universität Wien, 2022. DOI: 10.34726/hss.2023.57001 (cit. on pp. 18, 21).

[14] Daniel Neunteufel, Stefan Grebien, and Holger Arthaber. "Indoor Positioning of Low-Cost Narrowband IoT Nodes: Evaluation of a TDoA Approach in a Retail Environment." In: *Sensors* 22.7 (2022). ISSN: 1424-8220. DOI: 10.3390/s22072663. URL: https://www.mdpi.com/1424-8220/22/7/2663 (cit. on p. 21).

[15] Nuand. *bladeRF 2.0 micro block diagram*. July 2023. URL: https://www.nuand.com/product/bladerf-xa4/ (cit. on p. 23).

[16] C.K. Adithya Rangan et al. "Data Rate Based Performance Analysis and Optimization of Bulk OUT Transactions in USB 3.0 SuperSpeed Protocol." In: *2018 Second International Conference on Advances in Elec-*

tronics, Computers and Communications (ICAECC). 2018, pp. 1–6. DOI: 10.1109/ICAECC.2018.8479467 (cit. on p. 24).

[17] Jan Kunz and Petr Beneš. "VERSATILE CHIRP SINE GENERATOR ON FIXED-POINT FPGA." In: *Acta Polytechnica* 60.6 (Dec. 2020), pp. 462–468. DOI: 10.14311/AP.2020.60.0462. URL: https://ojs.cvut.cz/ojs/index.php/ap/article/view/6049 (cit. on p. 32).

[18] Chiara Falsi et al. "Time of Arrival Estimation for UWB Localizers in Realistic Environments." In: *EURASIP Journal on Advances in Signal Processing* 2006 (Dec. 2006). DOI: 10.1155/ASP/2006/32082 (cit. on p. 56).

[19] P.M. Djuric and S.M. Kay. "Parameter estimation of chirp signals." In: *IEEE Transactions on Acoustics, Speech, and Signal Processing* 38.12 (1990), pp. 2118–2126. DOI: 10.1109/29.61538 (cit. on p. 56).

[20] Achraf Mallat et al. "Statistics of the MLE and Approximate Upper and Lower Bounds–Part II: Threshold Computation and Optimal Pulse Design for TOA Estimation." In: *IEEE Transactions on Signal Processing* 62.21 (Nov. 2014), pp. 5677–5689. DOI: 10.1109/tsp.2014.2355776. URL: https://doi.org/10.1109%2Ftsp.2014.2355776 (cit. on pp. 59, 61).

[21] Daniel Neunteufel, Andreas Fuchs, and Holger Arthaber. "ToF-based Indoor Positioning for Low-power IoT Nodes." In: *2020 54th Asilomar Conference on Signals, Systems, and Computers*. 2020, pp. 641–645. DOI: 10.1109/IEEECONF51394.2020.9443431 (cit. on p. 65).